

Microelectrode Implants for Spinal Cord Stimulation in Rats

Thesis by

Mandheerej Singh Nandra

In Partial Fulfillment of the Requirements

for the Degree of

Doctor of Philosophy

California Institute of Technology

Pasadena, California

2014

(Defended on Sept 24, 2014)

© 2014

Mandheerej Nandra

All Rights Reserved

Acknowledgements

First and foremost, I must express my most sincere gratitude towards my advisor, Prof. Yu-Chong Tai. Your depth of knowledge and sheer brilliance have guided and inspired me throughout my time at Caltech, and I will never forget your unwavering support for me through countless challenging times during this project, and the life lessons I have learned from you. It is truly my honor to be a part of your lab.

This dissertation could only be achieved with the dedicated effort from the Edgerton lab at UCLA. I am grateful that Dr. Reggie Edgerton has given me this opportunity to join in the effort to push the boundaries of spinal cord research. I am forever in debt to the tireless work ethic of Parag Gad and Dr. Jaehoon Choe for their work with the animals used in this study and their concise analysis.

I would like to thank my various colleagues through the years at the Caltech Micromachining Lab. None of the work in this thesis would be possible without Dr. Damien Rodger's work in developing microelectrode fabrication technology at our lab. Dr. Angela Tooker and Dr. Wen Li were excellent mentors in teaching me all I needed to know in the lab. Thank you, Dr. Luca Giacchino and Dr. Ray Huang, for your friendship as we progressed through Caltech together. And to Dr. John Chen, Dr. Justin Young-Hyun Kim, Dr. Wendian Shi, Dr. Charles Deboer, Zhao Liu, Dongyang Kang, Yang Liu, Shell Zhang, and Nick Scianmarello: it was a privilege working alongside you all.

A special thank you goes out to Dr. Yu Zhao of our lab for being an amazing lab mate and friend. I felt like every time I sat down to teach you something, I learned just as much in return, and will cherish all the discussions we had about science and life. Your warm spirit and exuberant energy have never failed to put a smile on my face.

I am also grateful to Christine Garske for being so kind and helpful to both me and the rest of the lab with purchases and administration. Many thanks to Mr. Trevor Roper for his relentless work in keeping the lab equipment running smoothly.

Finally, I wish to extend my most sincere thanks to my family. I cannot thank my parents enough for the support and love they gave me throughout my life and guiding me to my passion for engineering. To my sister Dr. Sukhjeen Nandra and brother Dr. Kiritpaul Nandra, thank you so much for the many long and heartfelt conversations we had over the years. And to my future wife Amarjit, thank you for your endless love and support, and most importantly putting a smile on my face whenever I needed it. I love you all, and truly would not have completed this journey without you.

Abstract

Paralysis is a debilitating condition afflicting millions of people across the globe, and is particularly deleterious to quality of life when motor function of the legs is severely impaired or completely absent. Fortunately, spinal cord stimulation has shown great potential for improving motor function after spinal cord injury and other pathological conditions. Many animal studies have shown stimulation of the neural networks in the spinal cord can improve motor ability so dramatically that the animals can even stand and step after a complete spinal cord transaction.

This thesis presents work to successfully provide a chronically implantable device for rats that greatly enhances the ability to control the site of spinal cord stimulation. This is achieved through the use of a parylene-C based microelectrode array, which enables a density of stimulation sites unattainable with conventional wire electrodes. While many microelectrode devices have been proposed in the past, the spinal cord is a particularly challenging environment due to the bending and movement it undergoes in a live animal. The developed microelectrode array is the first to have been implanted in vivo while retaining functionality for over a month. In doing so, different neural pathways can be selectively activated to facilitate standing and stepping in spinalized rats using various electrode combinations, and important differences in responses are observed.

An engineering challenge for the usability of any high density electrode array is connecting the numerous electrodes to a stimulation source. This thesis develops several technologies to address this challenge, beginning with a fully passive implant that uses one wire per electrode to connect to an external stimulation source. The number of wires passing through the body and the skin proved to be a hazard for the health of the animal,

so a multiplexed implant was devised in which active electronics reduce the number of wires. Finally, a fully wireless implant was developed. As these implants are tested in vivo, encapsulation is of critical importance to retain functionality in a chronic experiment, especially for the active implants, and it was achieved without the use of costly ceramic or metallic hermetic packaging. Active implants were built that retained functionality 8 weeks after implantation, and achieved stepping in spinalized rats after just 8-10 days, which is far sooner than wire-based electrical stimulation has achieved in prior work.

Table of Contents

1. Introduction.....	1
1.1 Paralysis and Spinal Cord Injury	1
1.2 Spinal Cord Stimulation.....	3
1.3 Microelectrode Technology	5
1.3.1 Introduction to MEMS	5
1.3.2 Microelectrode arrays.....	6
1.3.3 Flexible Microelectrodes and Parylene MEMS	8
2. Microelectrode Array for Spinal Cord Stimulation	9
2.1 Introduction.....	9
2.2 Design Constraints	10
2.3 Fully Microfabricated Implant.....	11
2.3.1 Fabrication.....	13
2.3.2 Surgical Procedure	15
2.3.2.1 Headplug and EMG wires	15
2.3.2.2 Spinal cord transection and array implantation.....	16
2.3.3 Initial Results and Analysis.....	18
2.4 Wired Microelectrode Array Implant	19
2.4.1 Spinal baseplate.....	20
2.4.2 Epoxy and Silicone Encapsulation	21
2.4.3 Headplug design.....	23
2.4.4 Wire bundle design.....	24
2.4.5 Surgical Procedure	25

2.5	Optimization of Electrode Array	26
2.5.1	Electrode Delamination Prevention	27
2.5.2	Stress Relief Structure.....	29
2.5.3	Conductor Redundancy and Final Design.....	30
2.6	Results.....	32
2.6.1	Evoked Responses.....	33
2.6.2	Stepping.....	34
2.6.3	Animal Health Issues	34
2.7	Summary	35
3.	Multiplexed Microelectrode Array Implant.....	37
3.1	Introduction.....	37
3.2	Design Requirements	38
3.3	Multiplexed Implant System.....	40
3.3.1	Layout and Surgery	41
3.3.2	Multiplexed implant	42
3.3.3	Multiplexer Circuit.....	43
3.3.3.1	Multiplexer Circuit Operation.....	44
3.3.3.2	PCB Layout	45
3.3.4	Packaging	46
3.3.5	Control Box	48
3.3.6	Software	49
3.4	Results.....	51
3.4.1	Evoked Potentials.....	51

3.4.2	Stepping.....	53
3.5	Summary	55
4.	Wireless Multielectrode Array Implant	57
4.1	Introduction.....	57
4.2	Design Requirements	58
4.3	Wireless Power Theory.....	59
4.3.1	Linear Model Approximation.....	60
4.3.2	Wireless Power Efficiency Derivation.....	61
4.3.3	Wireless Power Efficiency Optimization.....	63
4.4	Wireless Power Implementation	65
4.4.1	High Q coils	65
4.4.2	Primary Power Amp.....	68
4.4.3	Power Delivery Control	69
4.5	Wireless implant	73
4.5.1	System Overview	74
4.5.2	Wireless Microprocessor Transceiver Circuit.....	75
4.5.2.1	Recording	76
4.5.2.2	Stimulation	77
4.5.3	Power Regulation Daughterboard	78
4.6	Results.....	79
4.7	Summary	83
5.	References.....	85

List of figures

Figure 2.1: Illustration of the fully microfabricated implant and EMG wires positioned into the rat	12
Figure 2.2: Photograph of the fully microfabricated implant	13
Figure 2.3: Microfabrication steps of the first iteration of the electrode array	13
Figure 2.4: Illustration of the use of a suture to pull the array into the spinal column.	17
Figure 2.5: The most damaged section of the explanted array	18
Figure 2.6: Electron micrograph of the explanted array	19
Figure 2.7: Illustration of the wired array implant and EMG wires positioned into the rat.	20
Figure 2.8: Top view of two candidate layouts of the spinal baseplate relative to the electrode array during spinal flexion.	21
Figure 2.9: Illustration of the wired array implant after implantation	22
Figure 2.10: 48-pin custom headplug	24
Figure 2.11: Photograph of the complete wired implant	25
Figure 2.12: Photograph during surgery just before the array is pulled in	26
Figure 2.13: Electrode delamination.	27
Figure 2.14: Effect of pulse testing on electrode condition	28
Figure 2.15: Typical electrode before implantation (left) and after explantation (right) when equipped with a grid structure.	29
Figure 2.16: Straight (left) and undulating (right) traces of explanted electrode arrays..	29
Figure 2.17: Final microfabrication procedure	31
Figure 2.18: Photograph of the final electrode array	31

Figure 2.19: Rat suspended in a jacket over a treadmill.	32
Figure 2.20: EMG responses obtained from two different stimulation combinations.....	33
Figure 2.21: Stepping patterns from two different stimulation combinations	34
Figure 3.1: Multiplexed implant system block diagram	40
Figure 3.2: Layout of the multiplexed implant after surgery	41
Figure 3.3: Photograph of the multiplexed implant	42
Figure 3.4a: Multiplexer circuit schematic	43
Figure 3.4b: Sample configuration of multiplexer to stimulate combination B8-C9	45
Figure 3.5: Manually routed high-density PCB design for the multiplexer circuit	46
Figure 3.6: The final PCB for the multiplexed implant	46
Figure 3.7: Stimulator circuit	49
Figure 3.8: Screenshot of software interface during operation	50
Figure 3.9: Comparison of EMG recordings	52
Figure 3.10: Middle response from evoked potentials.....	53
Figure 3.11: Stepping responses with different combinations.....	54
Figure 4.1: Simplified circuit for inductive power transfer	59
Figure 4.2. Linear model for inductive power transfer	60
Figure 4.3: Impedance transformation of the parallel load R_L into a series load R_{LS}	61
Figure 4.4: A plot of wireless power transfer efficiency.	65
Figure 4.5: Comparison of parasitic resistance between two 11 turn coils	66
Figure 4.6: Simulation of coil parasitic resistance.....	67
Figure 4.7: Primary amplifier schematic and photograph	69
Figure 4.8: Ideal wireless power delivery.....	70

Figure 4.9: Circuit to regulate power absorption by the secondary coil and simulation results.	71
Figure 4.10: Illustration of the wireless array implant after implantation, and photograph of the complete implant	73
Figure 4.11: Block diagram for the wireless implant system.	74
Figure 4.12: Schematic for the microprocessor transceiver circuit	76
Figure 4.13: Stimulator subcircuit	77
Figure 4.13: Daughterboard containing the power delivery control circuit.....	78
Figure 4.14: Rat with wireless implant prototype just under the skin	80
Figure 4.16: Software user interface showing voltage waveform recording.	82
Figure 4.17: Photograph of the wireless implant inducing hindlimb motion in a spinalized rat.	83

1. Introduction

1.1 Paralysis and Spinal Cord Injury

Paralysis is the loss of muscle function a part of the body. There are many causes of paralysis, but they can generally be classified as either spinal cord injury (SCI) or a disease of the spinal cord. The symptoms often include not only impaired motor function, but it can also affect autonomous systems like bowel movement, urinary function, sexual function, etc. There are approximately 5.6M cases of paralysis in the US, and approximately half of them report either highly limited movement or none at all [1].

Approximately half of SCIs in the United States are classified as complete [2], meaning that the spinal cord has lost the ability to transmit information across a segment within it, cutting off all functional communication from the brain to the nerves below the injury site and resulting in no sensation or voluntary control of motor function below the injury site. This usually results in either paraplegia or quadriplegia, depending on the site of injury.

Although in most cases the cord is not completely transected or even cut, it is significantly damaged by interruption of blood flow supplying one of its segments or through spinal contusion. Even though the vertebral column protects the cord, when trauma is sufficient to compromise this protective cage, the broken vertebrae can impinge on the cord and crush or destroy the axons within it very quickly, with continued loss of axons over time [3]. Approximately 55% of spinal cord injuries occur in young victims between 16 and 30 years of age, making it a disease to bear usually for the rest of their lifetime, and more than 80% of victims are males [4]. Impairment is usually permanent, although some cases of incomplete SCI can be recovered from.

It should be noted that the spinal cord is not just a conduit for signal to pass from the brain to the rest of the body. While it receives no input from the motor cortex below a complete injury, and sensations of touch are lost, the spinal cord can still have significant functionality. It is capable of significant reflex control and even motor processing of proprioceptive input without any input from the brain, even when uninjured [5]. This gives hope to victims of SCI that therapies can offer a significant improvement in their quality of life.

Many therapies have been attempted for victims of SCI. The foot-drop stimulator, where stimulation of the peroneal nerve is used to counteract the problem of foot drag, has seen mixed results [6,7]. More coordinated movements are difficult to control with peripheral nerve or muscle stimulators because they require precise timing and amplitude of stimulation along with many electrodes located in disparate parts of the body. While the surgical complications of the latter can be mitigated with skin surface electrodes, they are unable to target muscles with specificity. Simpler therapies such as treadmill training have proven to provide some degree of stepping [8] and weight-bearing standing [9] in felines with complete SCI, and it has been demonstrated that the same applies to humans [10]. It has been known that the spinal cord shows significant plasticity, so such adaptations are not entirely unexpected, and the concept of motor primitives [11,12] has been suggested as a basis for an injured spinal cord being capable of providing these basic locomotive functions. In theory, the backwards movement of the limbs as a result of locomotion (in these cases, due to the treadmill) provide proprioceptive feedback which can generate a reflex arc (usually controlled by the spinal cord's grey matter interneurons [13]) that can rhythmically activate coordinated bilateral motion in the limbs, even

without input from the motor cortex. Neural networks in the lumbosacral spinal cord known as central pattern generators (CPG) provide the characteristic alternating motor patterns of gait and even compensate for errors and obstacles [14,15], using only sensory information from the limbs [16, 17]. As these neural circuits are triggered by electrical signals from sensory nerves, it is therefore logical to hypothesize that spinal stimulation can be a mechanism for improving the activation of these locomotion circuits, and this is indeed the case. If sufficiently controllable, such a technique could offer significant locomotion ability to a victim of SCI.

1.2 Spinal Cord Stimulation

In several studies, rat and feline spinal cords were isolated from supraspinal control with a complete spinal cord transection (they are then referred to as *spinal* or *spinalized* rats/cats), and when facilitated pharmacologically and/or by epidural spinal cord stimulation, the animals produced locomotor-like patterns in the hindlimbs [18,19]. Ichiyama et al. [20] reported that epidural electrical stimulation of the spinal cord can induce rhythmic, alternating hindlimb locomotor activity in chronic spinal rats. Stimulation at the L2 spinal segment at frequencies between 30 and 50 Hz consistently produced successful bilateral stepping. Similar epidural stimulation at other spinal segments were less effective, e.g., epidural stimulation at the T13 or L1 evoked rhythmic activity in only one leg and stimulation at the L3, L4, or L5 produced mainly flexion movements as opposed to stepping. These studies clearly establish that both the specific site of stimulation and sensory feedback [21] is critical to effectively produce stepping.

In recent developments, completely paralyzed human subjects were implanted with a commercially available spinal cord electrode array and stimulation package originally designed for pain suppression [22]. A combination of stimulation of specific spinal segments near the S1 spinal level, sensory information from the lower limbs, and weeks of training was sufficient to generate full weight-bearing standing. Surprisingly, these subjects also recovered some voluntary control of movements of the toe, ankle, and the entire lower limb, but only when epidural stimulation was present. This obviously cannot happen with a complete lack of communication between the brain and the spinal cord, but no activity was detectable without stimulation. It appears that very weak excitation of descending axons are capable of activating spinal motor circuits if the lumbosacral interneurons and motoneurons are made more sensitive through spinal cord stimulation. Therefore even patients with complete spinal cord injury are offered hope of regaining a range of motor functions with the help of epidural stimulation.

To further develop this promising treatment, a more thorough knowledge of the mechanisms of spinal cord stimulation is necessary. Key to uncovering this knowledge is the ability to better control the specific sites of stimulation and observing the corresponding motor outputs.

1.3 Microelectrode Technology

1.3.1 Introduction to MEMS

The field of MEMS – micro-electromechanical systems – has its origins in the integrated circuit industry brought about by the inventions of the point contact transistor from Shockley, Bardeen and Brattain in 1947 and the earlier development of the first photopolymer in 1935 by Louis Minsk. Technological advances in photolithography then proceeded at an astonishing rate, allowing denser and denser patterns to be created and more sophisticated circuits. It soon became apparent that the advantages of continuous miniaturization extended beyond just purely electrical circuits, as pointedly illustrated in Richard Feynman’s famous 1959 talk entitled, “There’s plenty of room at the bottom”.

MEMS technology has since developed into a rich body of knowledge in design and fabrication of miniaturized structures with electrical, mechanical, chemical, biological, and other functionality. This fabrication is often referred to as “micromachining”, and techniques can generally be classified into two categories: bulk and surface micromachining, much like a sculptor uses subtractive and additive techniques in his art. In bulk micromachining, miniaturized structures are fabricated by removing a controlled pattern of material from a bulk, macro-sized substrate. In surface micromachining, thin layers of materials – ranging from hundreds of micrometers to sub-nanometer scale - are deposited on top of a substrate, and subsequently removed as necessary.

While there are a plethora of techniques in field of MEMS, there are a few key techniques relevant to the work of this dissertation. The two most common methods of depositing highly controlled layers of material are through physical vapor deposition

(PVD), and chemical vapor deposition (CVD). In PVD, a material that is vaporized in a vacuum condenses onto the target substrate, and is the most common method for depositing metals. Metals can be vaporized through resistance heating and electron beam heating, with the latter being necessary for high-melting point metals like platinum. In CVD, precursor materials usually in gaseous chemically react on the substrate to form a solid layer.

Of course, a simple stack of material layers can only produce a limited range of devices, so fundamental to all micromachining is the aforementioned photolithography, where a thin film of light-sensitive material known as photoresist is patterned by a projected image of light. Photoresist is usually (but not always) used as a temporary film that protects chosen areas from etchants, material deposition, etc. and it can then be dissolved to reveal the underlying material. Another key tool of both types of micromachining is plasma etching, where the ions in a plasma bombard exposed surfaces and selectively etch them away, depending on the exposed material. Variants of the process such as reactive ion etching (RIE) and deep reactive ion etching (DRIE) further expand the capabilities of the etching and types of structures that can be created.

1.3.2 Microelectrode arrays

Electrodes are a powerful tool in biology, enabling a researcher or health practitioner to inject current into living tissue and evoke a response. Implants featuring electrical stimulation of tissue have long been useful for treating human patients with a variety of ailments, with the most notable being the artificial cardiac pacemaker, which delivers electrical impulses to heart muscles in order to regulate the heart beat [23]. The

first implantable pacemaker was developed in 1958 [24], and implants using electrical stimulation have since been used for defibrillators [25], retinal prostheses [26], spinal cord stimulation, etc. As with many electronic devices, electrodes also benefit from miniaturization is apparent, as microelectrodes can localize the current injection source to a small area, and also offer the prospect being arrayed with high electrode density, offering precise spatial control of current injection.

The potential of miniaturizing electrode arrays was also seen in the 1950's, when insulated microwires were bundled to create an electrode array for studying neurons [27]. Microfabricated planar electrode arrays were first developed in the 1970's [28], and shank-like structures with electrodes [29, 30] were developed to penetrate the brain for neural recording, commonly known as the "Michigan array".

It may seem a misnomer to call a simple miniaturized electrode a MEMS device, as an electrode is simply an electrical interface between a metal and an electrolyte, whereas other bio-MEMS devices feature mechanical elements like channels, valves, cantilevers, pressure sensors, etc [31, 32, 33, 34]. However, the mechanical design of a microelectrode array is critical in its practical function. Tissue is a soft body, and in animals there is often substantial movement to be expected around the microelectrode, resulting in three major issues:

- A) Moving tissue can damage the electrode array if it is too fragile
- B) Moving tissue can be damaged or functionally impaired by mechanical reaction forces from the electrode array
- C) Moving tissue can create poor connections to the electrode

1.3.3 Flexible Microelectrodes and Parylene MEMS

An important innovation in addressing these issues was the development of *flexible* microelectrode arrays [35]. They originally used polyimide as a substrate, and allowed the implant to flex with tissue movement. Polyimide has since become a common material for flexible electrode devices, but another polymer by the name of Parylene has been used as a structural base for flexible implants, including all the microelectrode arrays used in the work of this dissertation.

Parylene is the trade name for a family of thermoplastic polymers, scientifically known as poly-para-xylylene. They were discovered in 1947 and commercialized by Union Carbide Corporation in 1965 [36], and while there are many varieties, the key variant for biomedical application is parylene-C, due to its Class VI biocompatibility certification from USP (United States Pharmacopeia) and approval for use by the FDA in various implants. There are some key advantages of parylene-C over polyimide, including pinhole-free conformal deposition and low permeability to water and ions [37, 38, 39]. These characteristics allow parylene-C films to be much thinner than an equally robust polyimide device, so despite having a higher Young's Modulus of ~4 GPa, they can result in more flexible devices. Gas-phase deposition is performed with the Gorham process, and results in conformal deposition of the film on a target at room temperature, which allows parylene-C to coat irregularly shaped devices.

Due to these strengths, parylene-C has been used in many bio-MEMs devices [40], including cochlear implants [41], neural prostheses [42], and in preliminary work for the subject of this dissertation, spinal cord implants

2. Microelectrode Array for Spinal Cord Stimulation

2.1 Introduction

Studies on spinal cord stimulation have made it clear that the intrinsic circuits of the spinal cord, if intact, are desirable targets for stimulus-based therapies and strategies. Moreover, the specific stimulation parameters are highly critical to the pattern and quality of functional motor output. In particular, the site of stimulation has been shown to be a key parameter affecting the motor output from stimulation [21]. One approach to improving the selection of stimulation sites quality is to use a high density microelectrode array [43]. Although stimulation occurs at the surface level, miniaturization of the electrode contacts limit the effective field of stimulation to a smaller area as compared to conventional wired surface electrodes. The specificity and high-density features of the electrode arrays enable them to capitalize on two key features of the spinal cord circuitries that are believed to be essential for rehabilitating posture and locomotion after spinal cord injury (SCI). Firstly, the spinal circuitry can be neuromodulated and the stimulation can be carefully delimited to affect only relevant areas of the spinal cord, thus optimizing the motor outcome. Secondly, as locomotor circuitries are highly plastic and adapt when provided with sensory cues during motor training [14], the density and versatility of the multi-electrode array allows for rapid adjustments of stimulation protocols and adaptations to physiological changes that may occur in the spinal cord over time after an injury.

Parylene C has emerged as an ideal electrode array substrate due to its biocompatibility, insulative properties, and flexibility (see previous section). The tear resistance of parylene C is large, making the arrays robust to surgical manipulation, as

well as to stresses produced in a moving animal [44]. The techniques needed to manufacture such microelectrode arrays are not new [45], but before the work of this dissertation, microelectrode arrays for spinal cord stimulation had only been used in an acute setting.

2.2 Design Constraints

A microelectrode array for epidural spinal cord stimulation in rats must meet many design requirements. First and foremost, the goal of the implant is to survive in the rat for a period of at least 4 weeks (and up to 8 weeks) with minimal degradation. This will allow biologists to obtain useful information about spinal cord injury, including the recovery of locomotion and the gradual progress of plasticity in the spinal cord as the rat is trained. This is a particularly difficult task due to the drastic movements seen in a live rat, which can induce major mechanical stresses in the device.

Of course, the implant must also be designed to avoid any deleterious effects on the rat. This not only requires careful material selection to avoid an adverse reaction in the rat, but also needs to be mechanically compliant enough to avoid causing damage upon movement. The width of the device must be chosen to be large enough that the electrodes have good lateral reach, but not so large that under movement the array damages the dorsal roots emanating from the spinal cord. It must be thick enough to keep functionality intact, but too thick of an array will reduce flexibility. Flexibility is also of critical importance to the microelectrode array, as the electrodes must maintain good contact with the spinal cord for effective delivery of stimulation, and the spinal cord's curvature changes with rat movement. Flexibility is also important in minimizing damage

to any tissue under movement and preventing the impairment of spinal cord functionality from undue pressure applied to it.

The multielectrode array must have the ability to interface with a stimulation source. Electrical connections passing through the skin are a potential source for infection, and wires passing through the body are a potential cause of internal tissue damage. While the ideal solution is to have a fully wireless implant, work towards that goal is discussed in Chapter 4. In the absence of such technology, the optimal location for electrical connections to pass through the skin has proven to be a headplug mounted on the skull. The implant must therefore be designed to cover the distance from the headplug to the spinal cord. This is a significant challenge, as our observations showed that the distance covered between the headplug and the region of interest on the spinal cord can vary from 6cm to 15cm, depending on the posture of the rat.

The experiment also requires EMG wires to be placed into the rat. This requires a pair of insulated wires with small openings to be inserted into each muscle under study. The signal obtained from these wires must also pass through a headplug. Anywhere from 4 to 8 muscles are of interest during stepping movement, corresponding to 8-16 additional connections to the head.

2.3 Fully Microfabricated Implant

Our first attempt at the implant involved microfabricating a combined structure of both the microelectrode array and a long cable section. Because most of the equipment at the Caltech Micromachining Lab handles wafers no larger than four inches in diameter,

the layout of the array and cable on the wafer is in a U-shape to obtain the necessary length. Figure 2.1 illustrates how the device is implanted into the rat:

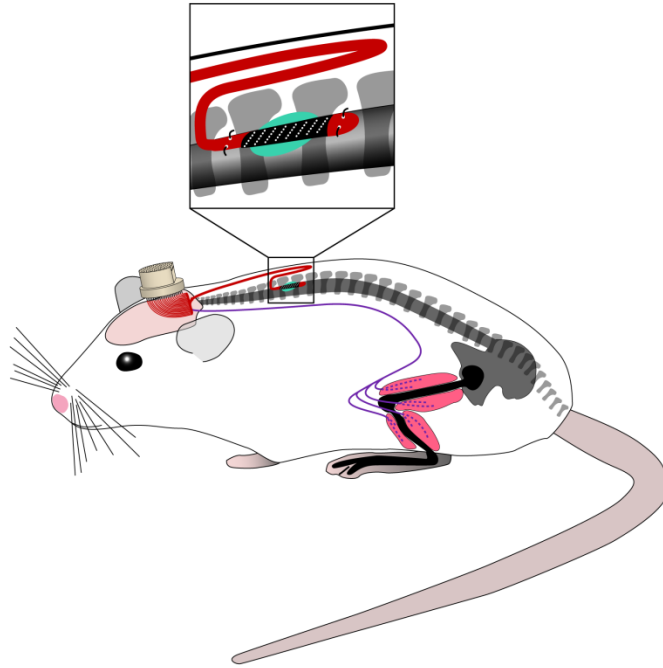


Figure 2.1: Illustration of the fully microfabricated implant and EMG wires positioned into the rat

As described in the introduction, the substrate for our microelectrode array is parylene-C. The structure essentially a parylene-platinum-parylene sandwich patterned and fabricated using lithography, as described in the following section. The headplug chosen for this initial design was the Omnetics Nano Series (model CON/16o25m-18P obtained from Plexon Inc), and provided 18 pins for connection to electrodes. The electrode array was arranged in a configuration of 2 columns and 9 rows, spaced so that the rows match up to the segments of the spinal cord as defined by the dorsal roots. Each electrode is circular with a diameter of $250\mu\text{m}$. The microfabricated structure is

interfaced to the headplug by applying conductive silver epoxy (CircuitWorks CW2400).

The complete implant is shown in Figure 2.2.

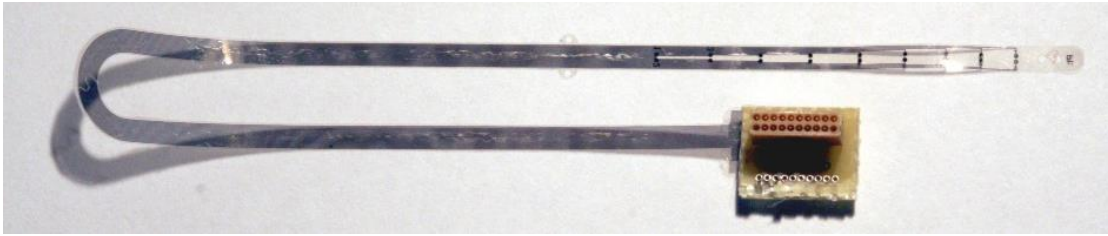


Figure 2.2: Photograph of the fully microfabricated implant

2.3.1 Fabrication

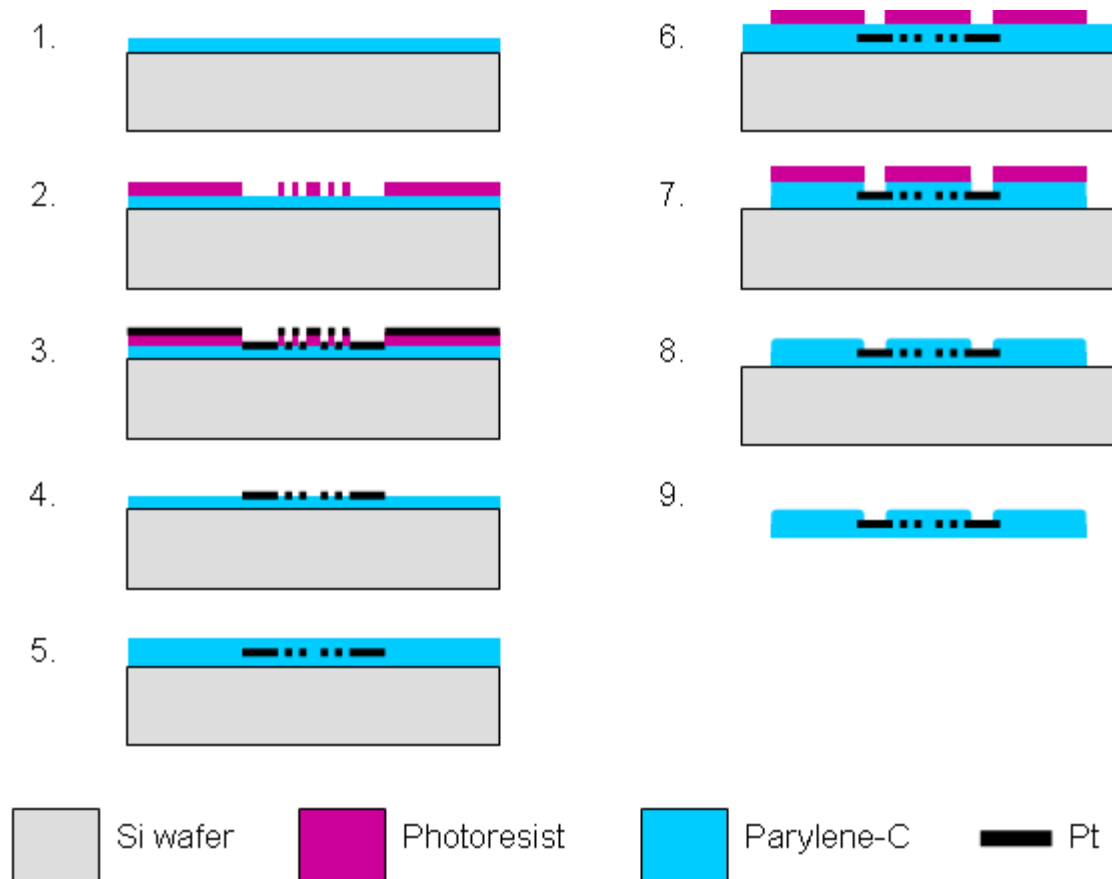


Figure 2.3: Microfabrication steps of the first iteration of the electrode array

The multielectrode arrays were fabricated as shown in the steps outlined in **Error! Reference source not found.** Approximately 5 μm of parylene C was then vapor deposited in a PDS2010 system (Specialty Coating Systems, Indianapolis, IN, USA) on the entire wafer. An LOR3B resist layer (Microchem Corp., Newton, MA, USA) and an AZ1518 photoresist layer (AZ Electronic Materials, Branchburg, NJ, USA) were spun on top of the parylene, exposed in a Kasper 2001 contact aligner (Kasper Instruments, Inc., Sunnyvale, CA, USA) and developed to achieve a liftoff pattern comprising contacts, conductive traces, and electrodes. After hard bake, approximately 2000 \AA of platinum was then e-beam evaporated (SE600 RAP, CHA Industries, Fremont, CA, USA) on the wafer. The subsequent photoresist strip generates the desired single-layer metallization pattern. An approximately 5 μm thick coating of parylene C is then deposited, followed by a spin coating of photoresist. This photoresist etch mask is exposed over the areas of the electrodes and contact pads and to pattern the overall array geometry, and the entire wafer is then subjected to an RIE in oxygen plasma, removing the parylene insulation over the electrodes and the parylene surrounding the array. The photoresist mask is then removed with solvent. The arrays are finally removed from the silicon by placing the wafer in a deionized water bath and peeling them from their edge. The water will then release the rest of the structure due to the hydrophobicity of the underlying parylene surface.

An annealing process in a Lindberg vacuum oven then follows. The arrays are placed between flat sheets of Teflon, loaded into the oven, and a small metallic weight is placed on top of the sheets to keep it together. The oven is evacuated to 10mTorr pressure and then heated to 200°C for a period of two days. It is critical that the arrays are not

exposed to any oxygen under elevated temperature, so a 6 hour cooling period is performed to ensure no section of the oven is over 100°C before venting. The annealing process helps the sandwich structure to form a better bond, as the parylene polymerization process does not chemically bond with previously deposited parylene exposed to air and the lithographic process.

2.3.2 Surgical Procedure

The surgical procedure involved fixing the array headplug to the skull, implanting the array inside the spinal cord, and transecting the spinal cord to induce lower body paralysis. A second headplug with EMG wires was also implanted, with the EMG wires fed through the body and inserted into leg muscles to monitor activity.

2.3.2.1 Headplug and EMG wires

To create a surface for the headplug, the muscles and fascia were retracted laterally from the skull after a small incision was made at its midline. Small grooves were made in the skull with a scalpel, and it was dried thoroughly. The array headplug and an Omnetics head connectors with Teflon-coated stainless steel wires (Cooner Wire AS632) were securely attached to the skull with screws and dental cement as described previously [46]. The medial gastrocnemius (MG), tibialis anterior (TA), and soleus (Sol) muscles were implanted bilaterally with EMG recording electrodes as described by Roy et al. [47]. Skin and fascial incisions were made to expose the belly of each muscle. Two ground wires were routed subcutaneously to each muscle. The wires were inserted into the muscle belly using a 23-gauge needle and a small notch (~0.5-1.0

mm) was removed from the insulation of each wire to expose the conductor and form the electrodes. The wires were secured in the belly of the muscle via a suture on the wire at its entrance into and exit from the muscle belly. The wires were looped at the entrance site to provide stress relief. The proper placement of the EMG wires were verified during the surgery by stimulating the appropriate channels of the headplug.

2.3.2.2 Spinal cord transection and array implantation

A partial laminectomy was performed at the T8-T9 vertebral level and a complete spinal cord transection to include the dura was performed at ~T8 spinal level using microscissors. Two surgeons verified the completeness of the transection by lifting the cut ends of the spinal cord and passing a glass probe through the lesion site. Gel foam was inserted into the gap created by the transection as a coagulant and to separate the cut ends of the spinal cord.

To implant the array, the spinous processes and portions of the dorsal and lateral aspects of the vertebra of T11, the rostral part of T12 and L4 were removed. A suture (4.0 Ethilon) was inserted through the opening at L4 and passed down to the opening at T11. This suture then was threaded into holes at the most caudal end of the electrode array, back into the opening at T11, and passed down to the first opening at L4. This suture was then able to gently pull the array rostrally between the dura and the vertebral column, as shown in Figure 2.4. The most rostral row of electrodes was placed at the middle of the T12 vertebra. Once the array was positioned satisfactorily over the dorsal surface of the

spinal cord, the rostral end of the array was sutured (using 8.0 Ethilon) to the dura to secure it in position.

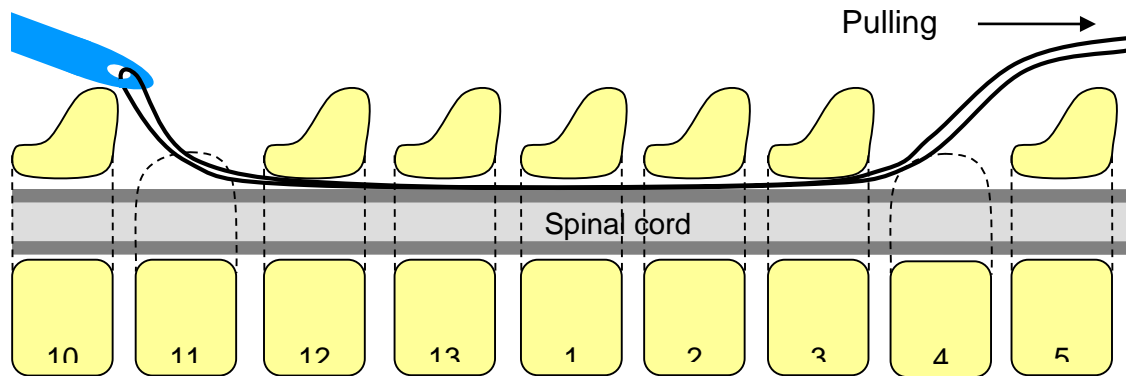


Figure 2.4: Illustration of the use of a suture to pull the array into the spinal column.

All incision areas were irrigated liberally with warm, sterile saline. All surgical sites were closed in layers, i.e., muscle and connective tissue layers with 5.0 Vicryl (Ethicon, New Brunswick, NJ) and the skin incisions on the back and the limbs with 5.0 Ethilon. All closed incision sites were cleansed thoroughly with warm saline solution. Analgesia was provided by buprenex (0.5–1.0 mg/kg, 3 times/day s.c.). The analgesics were initiated before the completion of the surgery and continued for a minimum of 2 days post-surgery. The rats were allowed to fully recover from anesthesia in an incubator. The spinal rats were housed individually in cages that had ample CareFresh bedding and their bladders were expressed manually 3 times/day for the first 2 weeks after surgery and 2 times per day thereafter. The hindlimbs of the spinal rats were moved passively through a full range of motion once per day to maintain joint mobility.

2.3.3 Initial Results and Analysis

After the rat had healed for one week, stimulation of the spinal cord through the implant was attempted. Unfortunately, none of the electrodes sites proved to be responsive at the initial testing or subsequent attempts. Using low frequency (1 Hz or slower) pulses, the rat should show a twitch movement in the legs even in the absence of rhythmic stepping, but none was observed. The implant was then removed to examine the mode of failure.

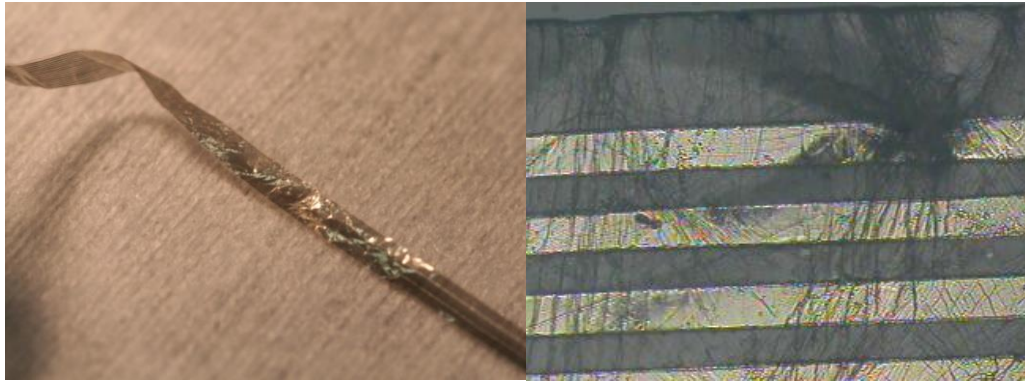


Figure 2.5: The most damaged section of the explanted array (a) under a microscope (b)

Upon removal of the implant, it was immediately apparent that the movement of the rat caused mechanical failure of the array. Figure 2.5 is a photograph of the explanted array, along with examination under the microscope. The wrinkles are clear evidence of the mechanical stresses that are placed on the array, and they were concentrated at the area where the array enters the spinal column. Figure 2.6 shows the most damaged areas under an electron microscope. The bending caused severe yielding and cracking of the parylene-C, and it can be reasonably concluded that this causes the platinum traces to break and lose connectivity between the headplug and the electrodes, as platinum can only withstand up to 3% elongation before breakage.

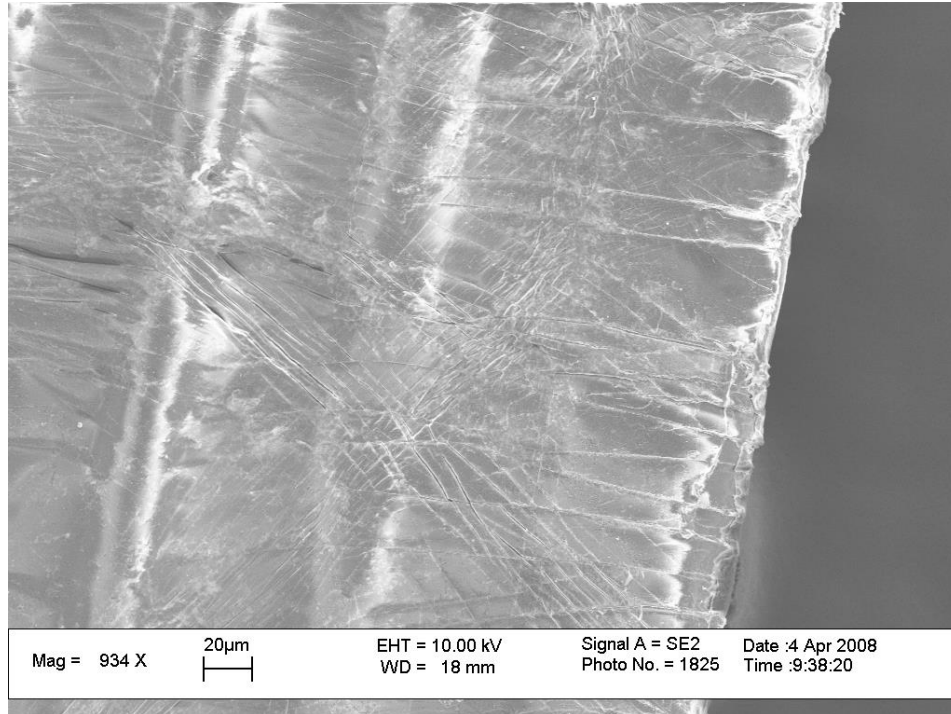


Figure 2.6: Electron micrograph of the explanted array

It was concluded that the design strategy of a fully microfabricated implant, i.e. using a microfabricated cable from the headplug to the spine, would be extremely difficult if not impossible to achieve.

2.4 Wired Microelectrode Array Implant

Owing to the failure of the fully microfabricated implant, it was clear that a different design strategy was required. Microelectrode technology clearly has a benefit in the ability to achieve high electrode density in the tight space inside the spinal column, and our surgical procedure can place the array in one motion. Without a microelectrode array, the only option is the use of many wires and individually suturing each one to the spinal cord using far more invasive surgery. However, the long cable section of the

microfabricated implant passing through the body has no advantage over wires aside from ease of fabrication, and a major disadvantage of being mechanically fragile. Therefore, a bundle of wires was incorporated into the design to bridge the connection between the headplug and the spine so that the microfabricated portion could be minimized (see Figure 2.7).

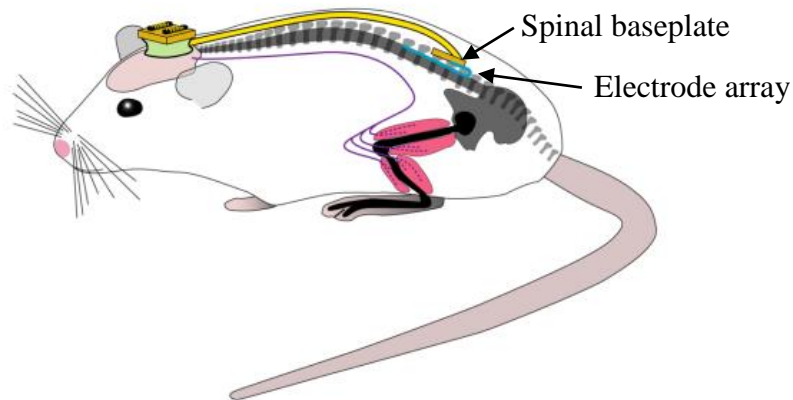


Figure 2.7: Illustration of the wired array implant and EMG wires positioned into the rat. The microfabricated portion is in blue and minimized.

2.4.1 Spinal baseplate

To maximize the success of the design, that there should be minimal movement of the microfabricated portion as it exits the spinal column. To achieve this, we designed a spinal baseplate that could be surgically anchored to the spine through the use of a fork shape that fits around a vertebra's spinous process, which is a bony protrusion on the dorsal side of each segment. The baseplate had an array of electrical vias so that wires can be soldered to one side and the array could be attached to the other side via conductive epoxy.

There was a choice of two configurations in the layout of the implant after surgery. The array could either make a U-turn or be kept as straight as possible. Although a straighter path may be a more natural position for the array, closer analysis suggests that when fixing the fork to the spinous process, spinal flexion during rat movement would likely result in more stress on the array, as illustrated in Figure 2.8. The U-turn keeps the fixation point of the fork just above the center of the electrode array, minimizing total deflection due to spine curvature. It was also determined that it would be somewhat more optimal for the array to enter on the caudal end at vertebra L4 (as opposed to the rostral end at T11), as there is less curvature of the spine in the lumbar region.

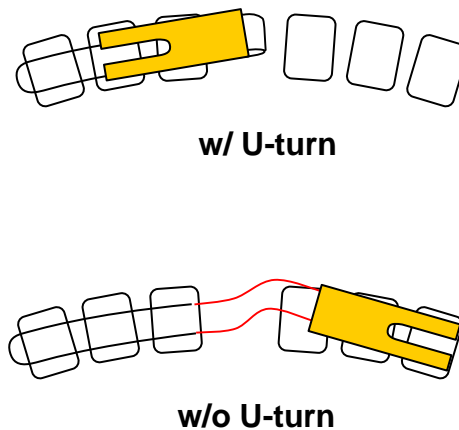


Figure 2.8: Top view of two candidate layouts of the spinal baseplate relative to the electrode array during spinal flexion. In red is the portion of the array theorized to undergo greater mechanical stress with the latter layout. The fork fits around the spinous process of a vertebra.

2.4.2 Epoxy and Silicone Encapsulation

A key factor in this implant design is the application of silicone and epoxy. After the electrode array is attached, the spinal baseplate is coated in biomedically compatible

epoxy (Loctite M-121HP) to insulate the electrode array interconnects from the body fluid. Epoxy was chosen for its rigidity, as silicone's elasticity could transmit mechanical stress to the silver epoxy interconnects and break the connections. However, silicone's elasticity is invaluable to provide a smooth transition from the rigid baseplate to the flexible array, as a sudden transition would create stress concentration at the junction between the two. Figure 2.9 illustrates the overall implant and encapsulation.

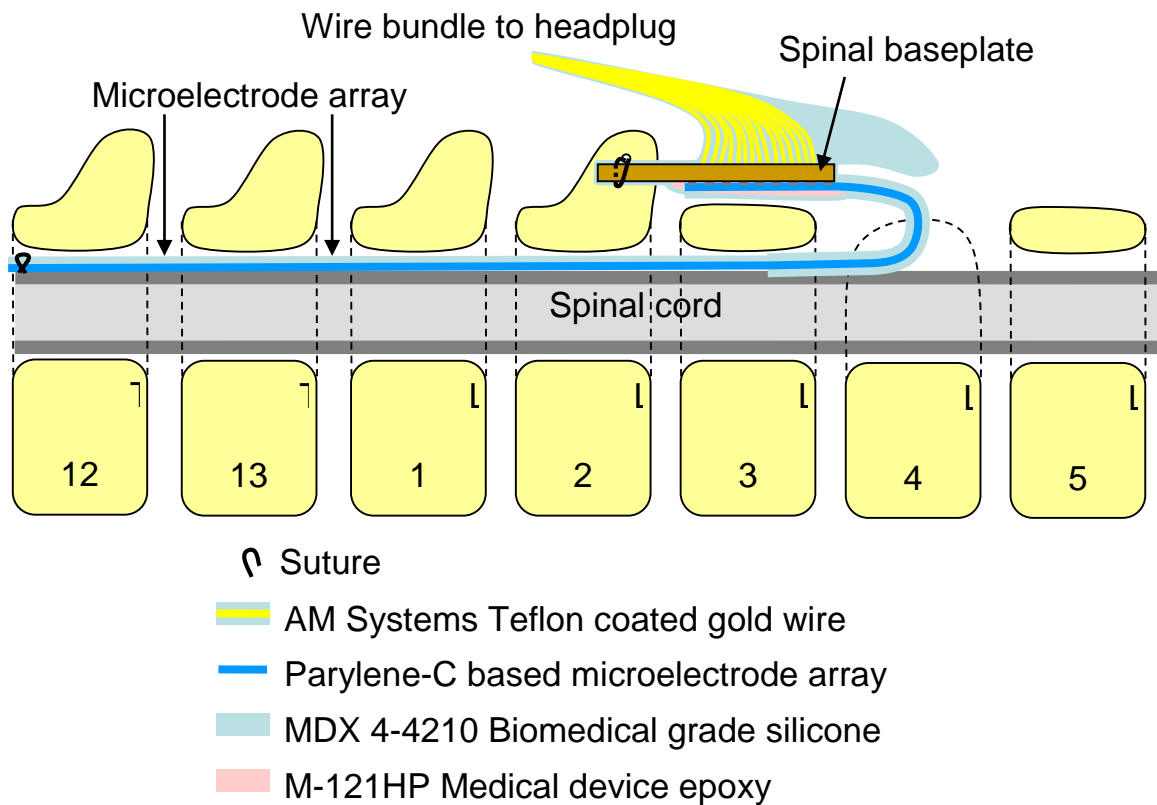


Figure 2.9: Illustration of the wired array implant after implantation

The Dow Corning MDX4-4210 silicone was chosen for its tested biocompatibility and consistency. It is strategically applied around the spinal baseplate to shield the array from soft tissue pressure, and also applied to the microelectrode array itself so that it will

be strengthened. The silicon coating helps prevent the array from bending very sharply and forming creases as we saw in the previous design. It was later found that if the silicon coating is too thick, it would apply pressure to the spinal cord and adversely affect the rat and the experiment, so a layer roughly 100 μ m thick was applied to as much of the microfabricated array as possible without covering the electrodes and retain flexibility. A solution of two parts uncured silicone to one part hexane was prepared to obtain a thin enough consistency such that after brushing the silicon on, the desired thickness was obtained.

2.4.3 Headplug design

The 18-pin Omnetics Nano connector used in the first implant's headplug was found to be cumbersome to assemble form electrical connections to (due to it's through-hole design), required significant force to mate, and didn't contain nearly enough connections for the desired number of electrodes and EMG wires. A 27 electrode array (9x3) was designed for this second generation implant to provide all the desired stimulation sites, so along with 8-16 EMG wires and two ground wires, up to 45 connections were needed. A custom 48 pin headplug was designed through the use of a PCB and two fine pitch SMT connectors (Panasonic F4S series, 24-pin), and can be seen in figure 2.10.



Figure 2.10: 48-pin custom headplug

2.4.4 Wire bundle design

Due to the large number of wires in the wire bundle for the electrode array, thin single stranded 75 μ m gold wires were used as opposed to the 15 strand stainless steel EMG wires. Gold wires were found to be optimal due to gold's ductility and flexibility along with ease of solderability. The wire bundle was also coated in silicone to prevent any sharp kinks for forming that could potentially break the wire. The complete wired implant, including the headplug, EMG wires, wire bundle, spinal baseplate, and electrode array is shown in figure 2.12.

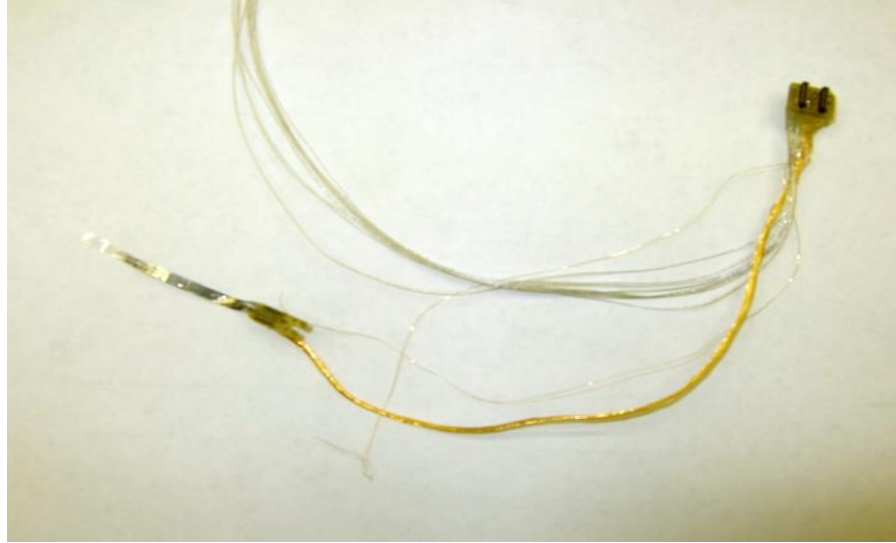


Figure 2.11: Photograph of the complete wired implant

2.4.5 Surgical Procedure

The surgical procedure for the wired implant was similar to that described in section 2.3.1, with the head plug and EMG wires implanted in the same way. However, a modification was made to integrate the addition of the spinal baseplate. Before inserting the array, The L3 spinous process was removed to form a flat surface, as seen in figure 2.11. The fork on the spinal baseplate of the implant was secured into the L2 spinous process, i.e., a suture (4.0 Ethilon) was threaded through the hole on the baseplate and tied around the L2 spinous process.

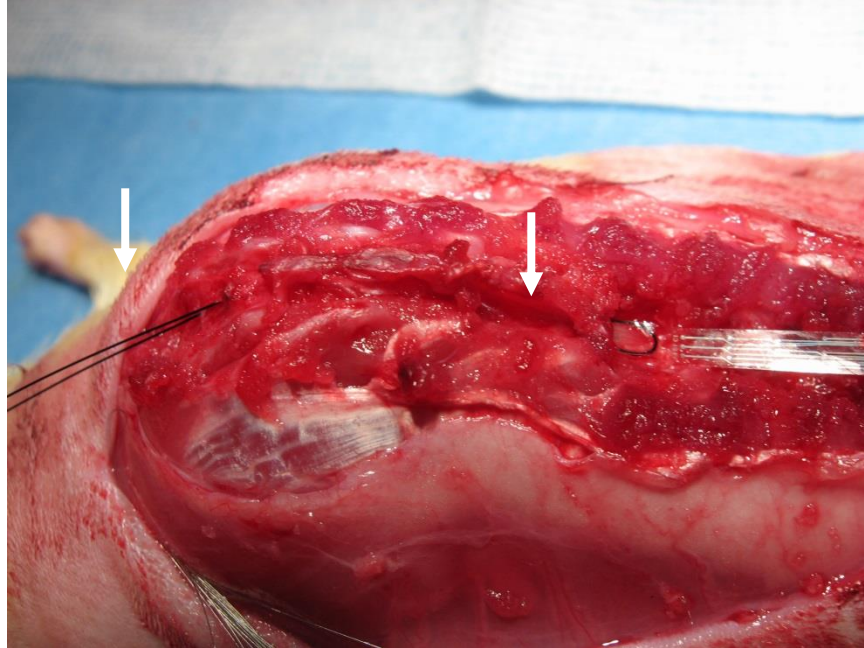


Figure 2.12: Photograph during surgery just before the array is pulled in

The orientation of the spinal baseplate required the array to be inserted in the opposite direction as described in section 2.3.1.1. Figure 2.12 is a photograph of the array just before being drawn into the spinal column with sutures. The suture was inserted through the opening at T11 and passed down to the opening at L4. This suture then was threaded into holes at the most rostral end of the electrode array, back into the opening at L4, and passed down to the first opening at T11.

2.5 Optimization of Electrode Array

While stimulation was achieved with the second generation implant, some of the electrodes would fail after some time. There are two main categories of individual electrode failure: mechanical failure of the trace going from the electrode to the

baseplate, and failure of the electrode itself through delamination. Various design iterations of the electrode array addressed these issues to improve longevity inside the rat.

2.5.1 Electrode Delamination Prevention

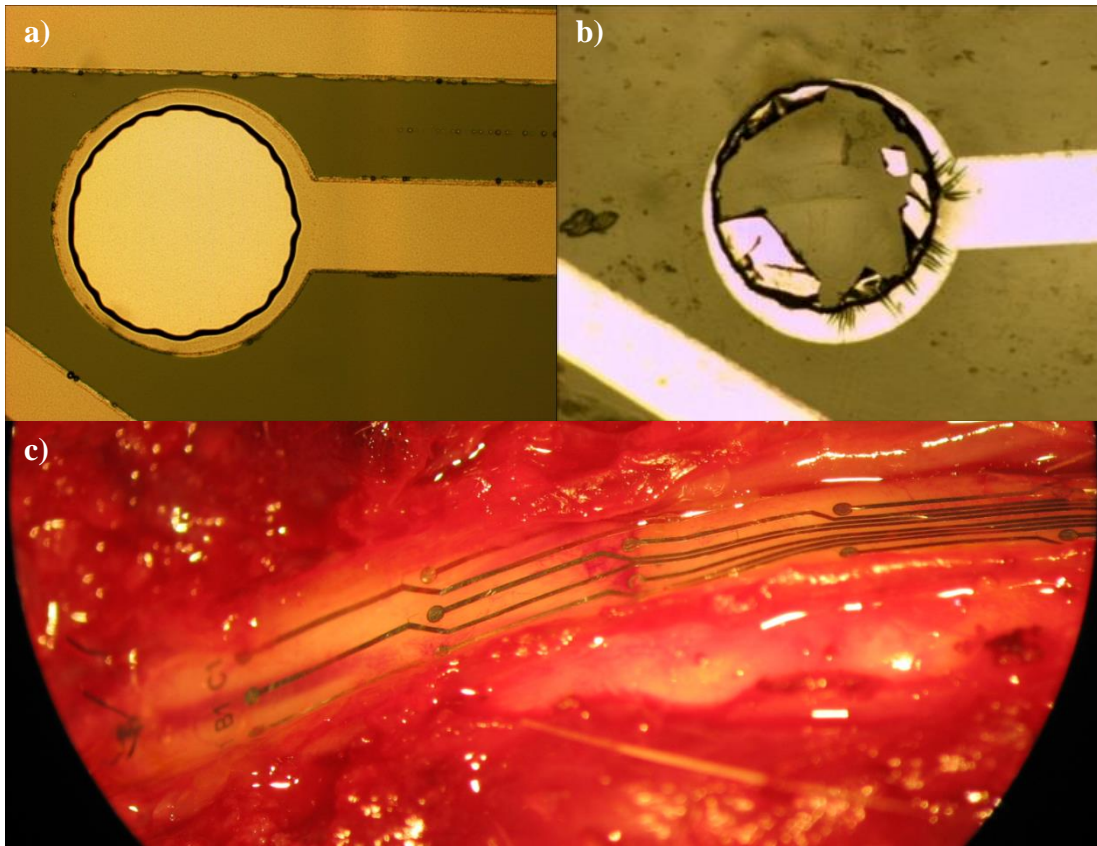


Figure 2.13: Electrode delamination. a) Typical electrode before implantation. b) Some electrodes after explantation showed degradation c) View of an electrode array on the dura of the spinal cord after 4 weeks in vivo, showing delamination.

Electrode delamination has long been a mode of failure for microelectrode arrays in vivo. Initially, we found anywhere from 1 to 7 electrodes out of 27 would undergo significant delamination, as seen in Figure 2.13. Lab tests showed that delamination was not a problem after 3 million pulses (5V amplitude and 1ms duration) were passed through the electrodes while soaking in saline, as seen in figure 2.14. From this, and

because the remaining electrodes mostly did not show any delamination at all despite being identical prior to implantation, we hypothesize that it is mechanical stress combined with chemical processes and electrical stimulation that causes delamination in vivo.

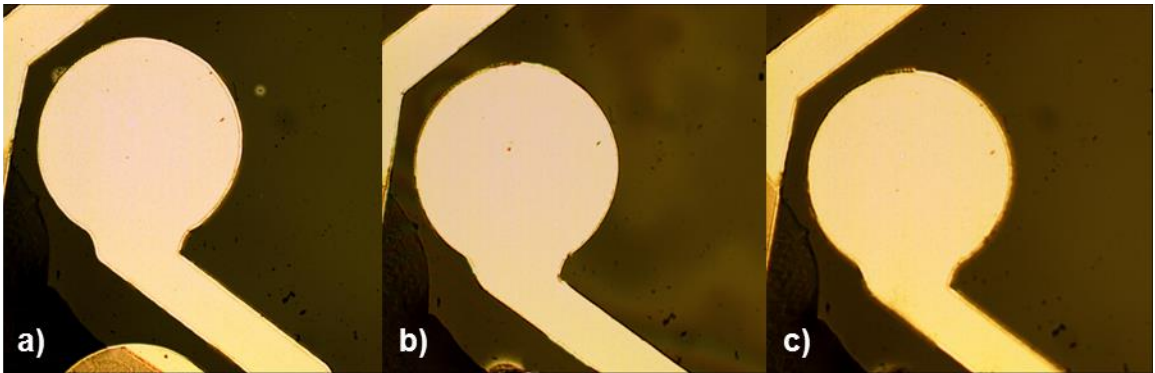


Figure 2.14: Effect of pulse testing on electrode condition after a) zero pulses, b) 1 million pulses, and c) 3 million pulses

To solve the problem of delamination, we used a two prong approach. First, we deposited a thin 100Å layer of titanium prior to the platinum deposition. Titanium is known to function as an adhesion layer during metal deposition. Secondly, we designed a grid structure over the electrodes, as seen in figure 2.15. The electrodes proved to remain intact after explantation, but show ripples that appear to suggest the onset of delamination. In fact, this is actually a product of the explantation process, in which a block of tissue containing the implant was excised from the terminated rat and soaked in ~5M sulfuric acid to dissolve the tissue. When a non-implanted electrode was exposed to the same process, it resulted in similar ripples. The grid and Ti adhesion layer proved sufficient to prevent delamination from occurring again.



Figure 2.15: Typical electrode before implantation (left) and after explantation (right) when equipped with a grid structure.

2.5.2 Stress Relief Structure

A stress relief structure was designed for one iteration of the electrode array, in which the traces from the electrodes to the pads were of an undulating form. Unfortunately, this structure did not improve the longevity of the array, as almost all the electrodes failed to stimulate after one week of implantation. Figure 2.16 compares the condition of straight and undulating traces after explantation. While the straight traces do show stress lines, the undulating ones proved to have more severe cracks. It is evident that the curvature of the undulations provide regions of stress concentration. From these areas, cracks in the parylene initiate and then propagate to the traces.

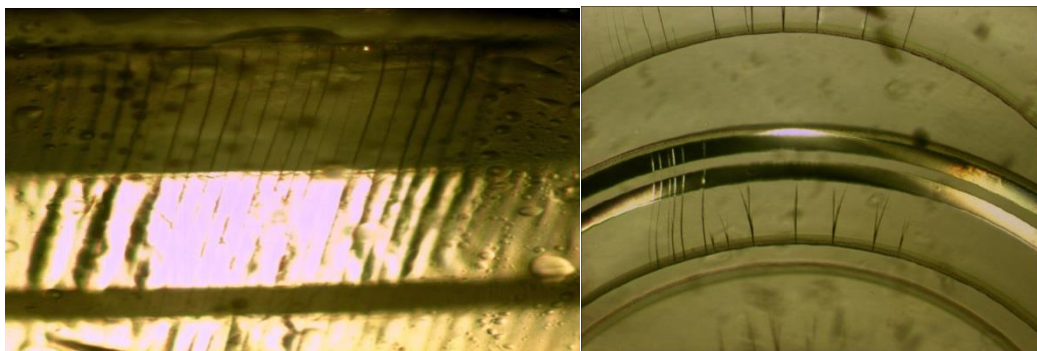


Figure 2.16: Straight (left) and undulating (right) traces of explanted electrode arrays

2.5.3 Conductor Redundancy and Final Design

Since the stress relief structures proved to be detrimental to array longevity, the final revision of the array made use of two traces per electrode. To maximize the effectiveness of this strategy, it is desirable for these two traces to be located far from each other so that localized damage to one part of the array would not affect both traces for any electrode. In order to accommodate the number of traces for such a design, the electrode orientation was changed from round to rectangular, offering more room between the electrodes for traces while retaining surface area.

One more modification to the array was the addition of a thick frame. As the failed undulating design showed, failure of the traces is often caused by cracks initiated near an edge that propagate through the material. To prevent this initial crack formation, a 10 μ m frame layer was added to the beginning of the fabrication process. Figure 2.17 shows the final overall fabrication process, and the final microelectrode array is shown in figure 2.18.

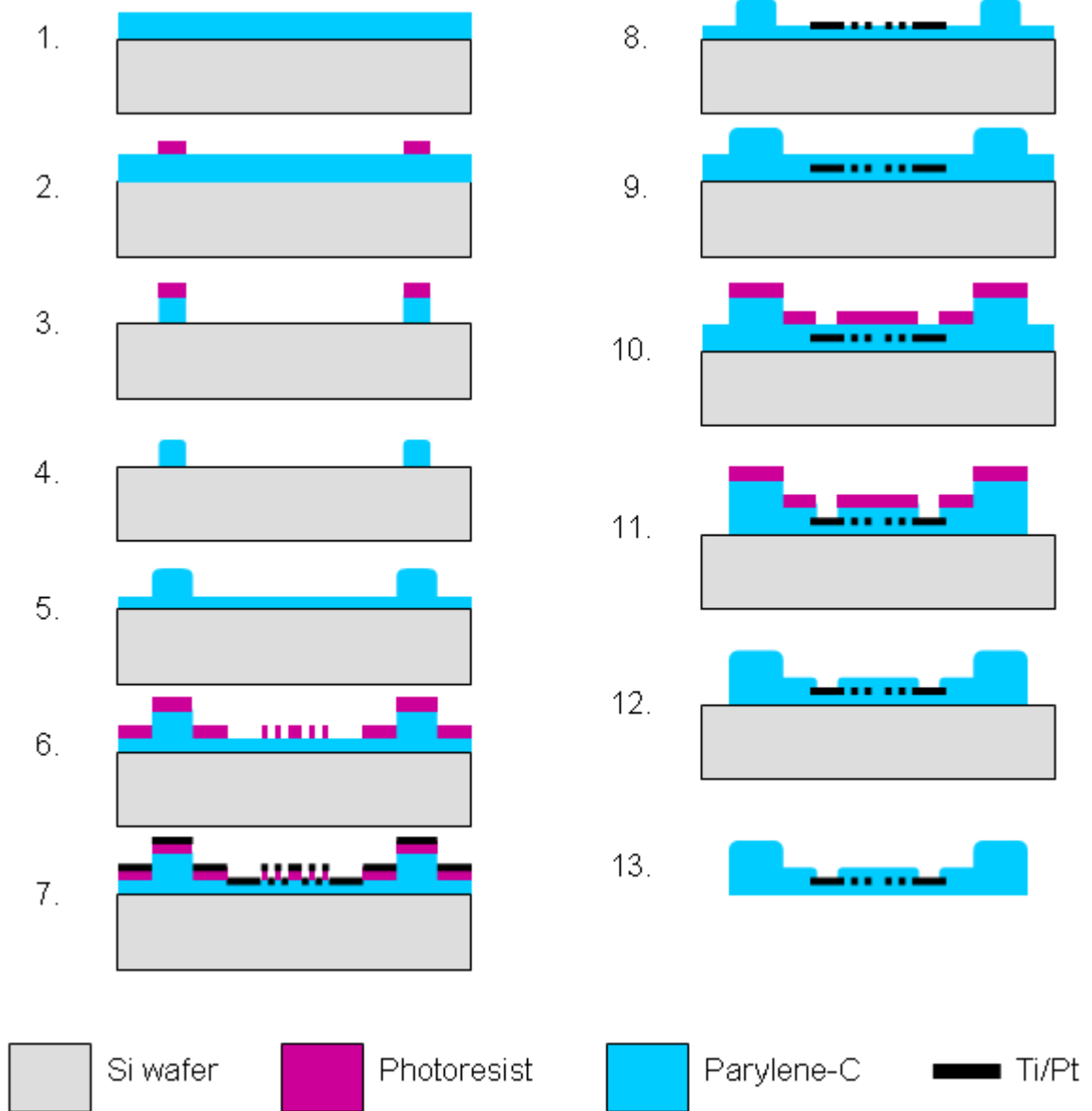


Figure 2.17: Final microfabrication procedure



Figure 2.18: Photograph of the final electrode array

2.6 Results

The wired implant was able to survive chronic implantation and stimulate the rat, with progressive electrode iterations reducing electrode failure count. Two different types of stimulation experiments were performed on the rat. One involves applying low frequency (typically 0.3-1 Hz) stimulation pulses of 0.5ms duration to evoke single responses in the leg muscles that show up in the EMG recordings. The other is a stepping experiment, where the rat is placed over a treadmill in a jacket (see figure 2.19 and [48]) and high frequency (typically 40Hz) stimulation invokes a stepping motion as the treadmill is run. Both experiments provide useful data for understanding the neural mechanisms of the spinal cord.



Figure 2.19: Rat suspended in a jacket over a treadmill.

2.6.1 Evoked Responses

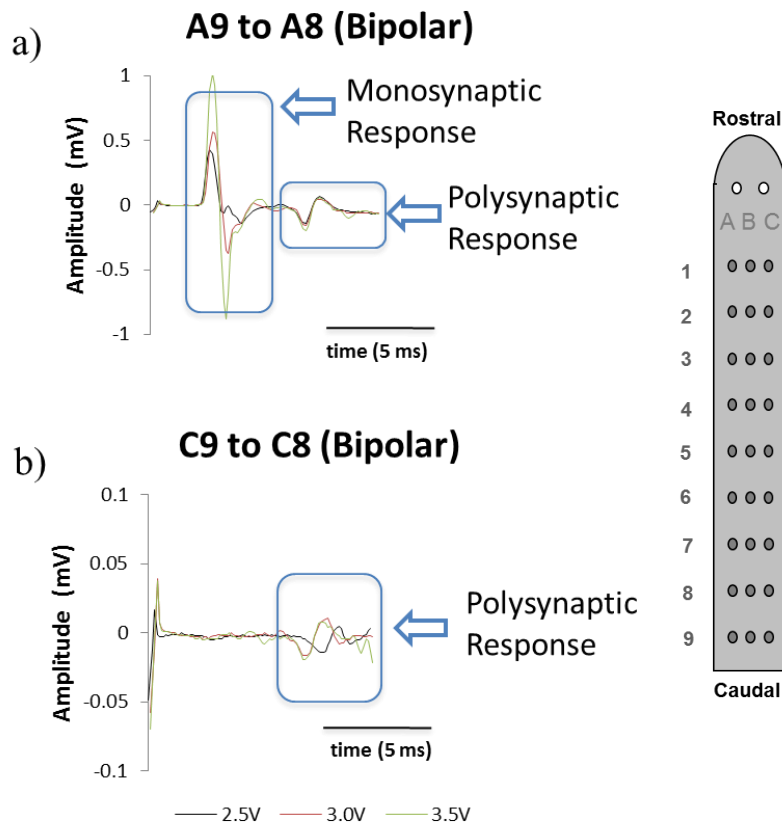


Figure 2.20: EMG responses obtained from two different stimulation combinations. The electrode naming convention is shown on the right.

By stimulating different combinations of electrodes, different types of waveforms were seen in the EMG recordings. Figure 2.20 is an example of such differences. When the A9-A8 combination was stimulated, both a monosynaptic and polysynaptic response was observed in the EMG recording. When the C9-C8 combination was stimulated, only a polysynaptic response was observed. Such observations give insights into the neural circuitry present inside spinal cords and their connections to muscles.

2.6.2 Stepping

Stepping was observed 8-10 days after the rats were spinalized. This is a key improvement over conventional stimulation using wire electrodes, which have generally taken 3 weeks or more for electrical stimulation alone to induce stepping. The reasons for this is unclear, but because stepping in early stages does not occur with every combination, it is likely that the better site specificity of an electrode array can have greater success in activating the spinal circuits.

Again, it was found that different stimulation combinations can invoke different biological responses. Figure 2.21 shows a stick-diagram representation of stepping patterns from two different stimulation combinations, as captured by a motion capture system.

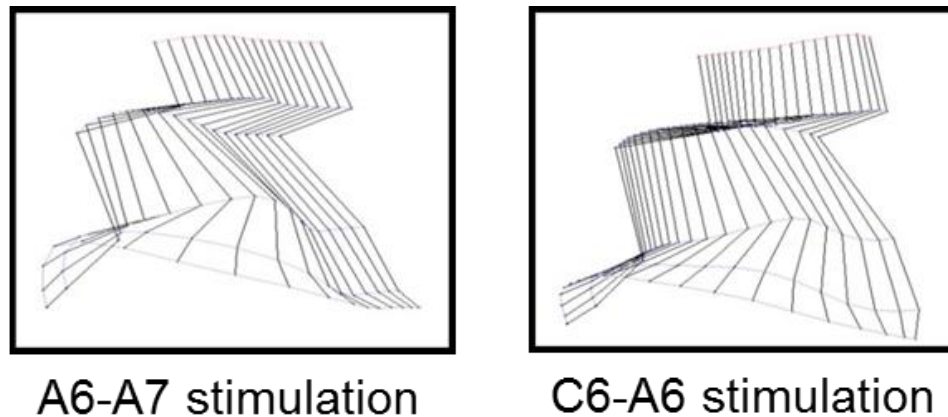


Figure 2.21: Stepping patterns from two different stimulation combinations

2.6.3 Animal Health Issues

A total of 22 rats were implanted with microelectrode implants as they went through the design iterations needed to arrive at the solution described in preceding

sections. Early designs of the implant had high failure rates, but even when the implant design was refined to be more robust, various health issues were still often seen in the rats. Some of these issues are known to happen on occasion for this type of experiment, such as rats chewing their paralyzed legs, but one issue in particular was related to the wired implant design.

For three of the animals, the wire bundle was found to rub against the underside of the skin. Since movement of the rat can change the distance between the headplug and spine by greater than a factor of 2, the wire bundle needed to be long enough to form a loop under the skin. This loop would sometimes form a kink after days inside a moving rat, and that kink could then rub on the skin enough that it would eventually protrude through. Infection was then inevitable, and these rats had to be terminated.

2.7 Summary

Through evolutionary design iteration, we have designed the first microelectrode array implant for spinal cord stimulation in rats that is capable of surviving in vivo for up to a month with minimal loss of functionality. To achieve this goal, we found that the implant design must minimize exposure of the microfabricated portion to mechanical stress, particularly, the point where it exits the spine. A novel baseplate structure achieves this by forming a rigid connection to a spinous process and interfacing the microelectrode array to a wire bundle. A surgical procedure was developed to slide the electrode array into the spinal column, allowing many epidural electrical contacts with only two laminectomies.

This was the first microelectrode array to be chronically implanted and achieve stepping in spinalized rats. Moreover, stepping was observed much sooner than had been seen before with conventional wire electrodes. The value of having a high number of stimulation sites was illustrated through varying biological responses depending on the sites chosen to stimulation. Depending on the combination of electrodes used, marked differences were seen in the EMG responses, both in terms of amplitude and ratio of monosynaptic and polysynaptic waveforms. Stepping patterns also varied with different stimulation combinations, showing different characteristics in the varying parts of the stepping cycle.

While these observations clearly illustrated the potential of high density electrodes to further study of spinal cord injury and develop effective therapies, complications arising in some rats during the surgery also suggested that a passive wire bundle is not necessarily the best way to interface between the electrodes and the stimulation source. The thickness of the wire bundle proved to be a health risk for the rat, on multiple occasions breaking through the skin over a period of weeks and necessitating termination of the experiment. A solution to this issue is highly desirable.

3. Multiplexed Microelectrode Array Implant

3.1 Introduction

In the previous chapter, our work clearly established the value of high density electrode arrays for spinal cord stimulation [49], but it also found significant health risks associated with having a high number of wires passing down the neck from the headplug to the spinal cord. It is important to address this issue to not only for a higher success rate with this 27-electrode experiment, but also to lay the foundation for a higher electrode count in future studies.

One possible solution to this issue is to use thinner wires, but the wires used in the previous chapter were already known to be thin enough that a risk of wires breaking over the duration of the experiment is a possibility. Taking this possibility to the extreme, a microfabricated cable could shrink the wire bundle substantially, but such an approach had already failed in our initial design, and was judged to have little chance for success with design iterations. The movement of the rat in the region between the spinal cord and headplug is too severe for a relatively fragile microfabricated cable or very fine wires, and past experience suggests that the skull must be used for electrical connections passing through the skin in a chronic experiment.

The logical deduction is that there must be a reduction in the number of wires passing down the body from the skull, and preferably no wires at all. In order to achieve this without reducing the number of electrodes, active electronics must be incorporated inside the implant while also remaining inside the financial limitations of the study. The ideal solution is to create a fully wireless electronics package capable of generating stimulation waveforms to the desired electrodes and recording all resulting responses. As

such a design would require substantial engineering effort, an intermediate solution was identified where a multiplexer circuit would allow many electrode sites to be addressed using far fewer wires. Such a circuit would necessarily be part of an eventual wireless design, because a design without multiplexing would need a separate stimulator circuit for all 27 electrodes, and would not be small enough to implant in a rat.

A major engineering challenge with active electronics in implants is the need to hermetically seal the electronics from bodily fluids while also being biocompatible. Typically, this is done with a biocompatible metallic or glass case, and electrical connections use ceramics as insulation which are covalently bonded to the case to prevent leakage. Such a case, unfortunately, is not commercially available for the size constraints of the rat and high number of electrical connections for the electrode array, and developing such a case is well beyond the financial resources of this work.

3.2 Design Requirements

The multiplexer circuit must be able to route the desired stimulation signal, and thus must handle a minimum voltage range of 10V. Up to 20V is desirable, as it was found in previous experiments that such voltages can be useful for obtaining responses if lower voltages do not work. To further reduce the number of wires, it must also route signals from the desired EMG wires to differential preamplifiers.

The circuit is designed to operate in 4 modes to meet the experimental requirements:

- A) stimulation between almost any two spinal electrodes, between any EMG wire pair, or between one spinal electrode and a body ground wire

- B) recording of 4 EMG signals, selected from 8 EMG wire pairs
- C) recording between almost any pair of electrodes on the spinal cord
- D) recording from 4 electrodes in the same column with respect to the fourth (e.g., A1-A9, A3-A9, A5-A9, and A7-A9).

Modes A and B are the primary objectives, while modes C and D are reserved for future investigation. The ability to stimulate EMG wires (in mode A) is needed to check position of EMG implants during surgery, as a stimulation pulse will make the muscle twitch if placed correctly.

The entire circuit must fit in the rat adjacent to the spinal cord much in the same way as the baseboard of the wired implant (described in section 2.4) so that the surgical procedure can remain the same. As such, the maximum dimensions are roughly 40x15x10 mm, as a larger package would present difficulties in placing the implant close to the spine in a manner similar to that described in section 2.4.5, which is a necessity to minimize damage to the electrode array.

This design must use off-the-shelf components only, as custom IC design is costly and time consuming. Finally, it is preferable for the circuit design to take into consideration the goal of fully wireless functionality in the future.

3.3 Multiplexed Implant System

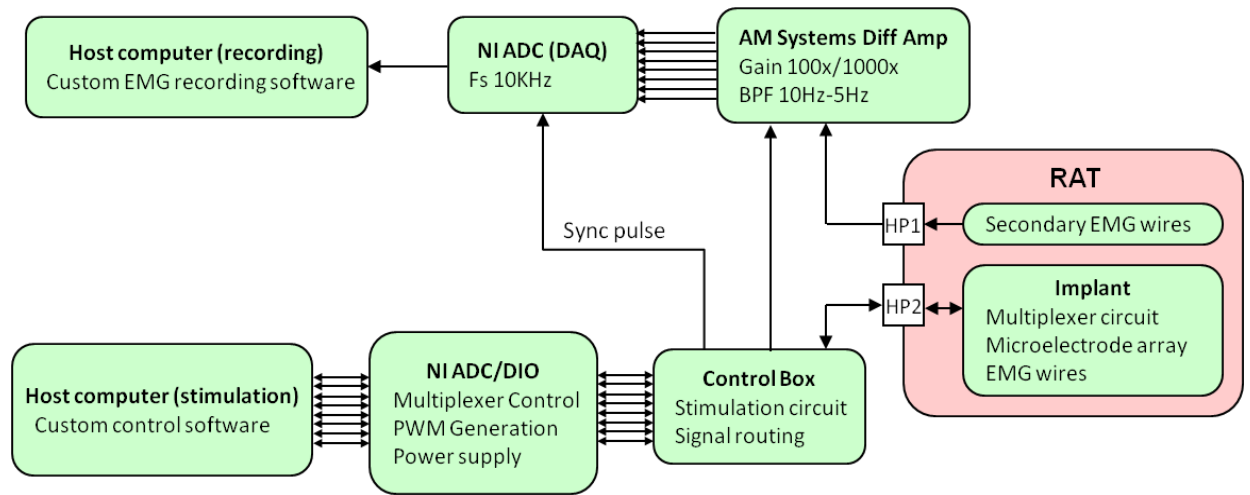


Figure 3.1: Multiplexed implant system block diagram

Figure 3.1 illustrates the overall system block diagram, and can be divided into two main sections. In the top half of the figure is the base recording system used with previous stimulation studies [50], and it was kept unchanged to leverage existing hardware and software infrastructure for EMG recording and analysis. This includes LabVIEW software, an ADC, and a multichannel EMG amplifier (AM Systems Model 1700). The bottom half of figure 3.1 shows new external components added needed to control the multiplexer. A second host computer with custom software is used to control the stimulation and multiplexer. This computer is connected to a DIO/ADC box (National Instruments PXI-6123), which is in turn connected to a control box. This box contains the stimulator circuit as well as interfacing between the ADC, the EMG amplifier, and the multiplexed implant. Power is also supplied to the implant by the control box.

Also illustrated at the right of figure 3.1 are the connections to the rat. HP2 is the headplug containing all signals from the multiplexed implant, and HP1 is a second

headplug containing secondary EMG wires. The latter was not used in all rats, but when used with EMG wires placed in the same muscles as EMG wires placed in the implant, it allowed verification that the multiplexer circuit did not fail to record EMG signals (see section 3.4.1 and figure 3.9 for results).

3.3.1 Layout and Surgery

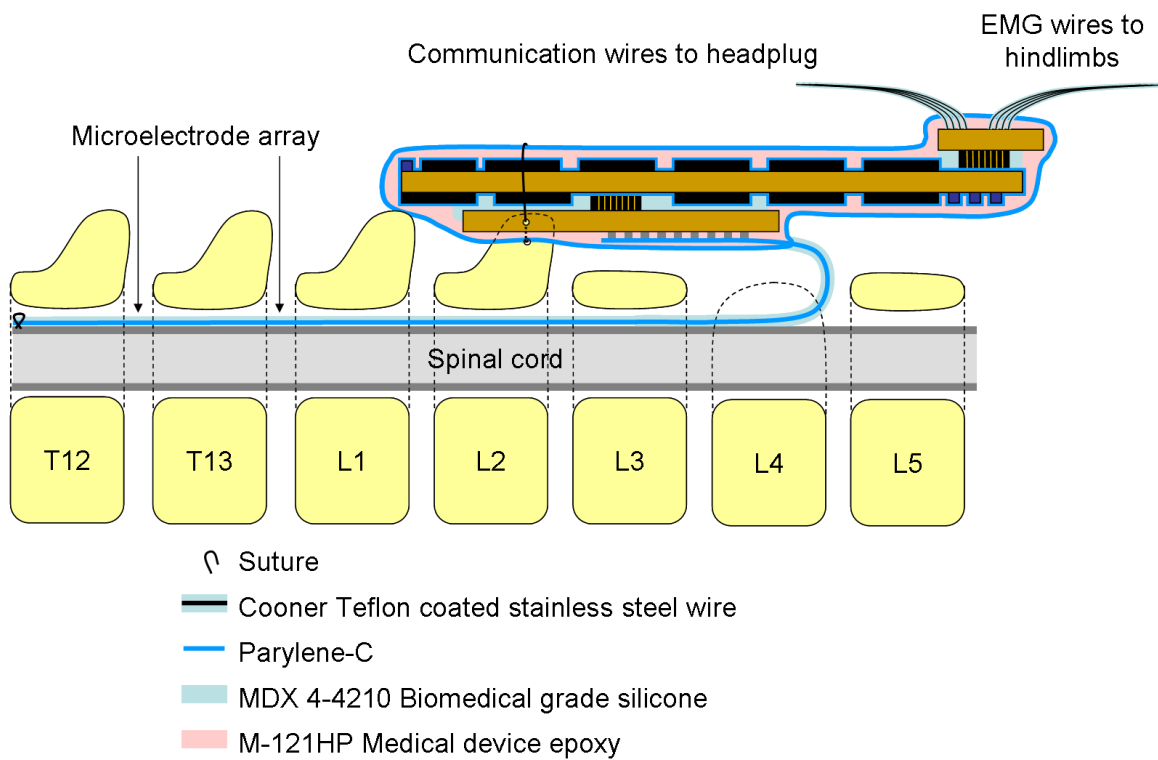


Figure 3.2: Layout of the multiplexed implant after surgery

The layout of the multiplexed implant after surgery can be found in figure 3.2. It is similar to that of the wired implant in figure 2.9, but the spinal baseplate is now enlarged into an electronics package. In addition, EMG wires originate from the implant as opposed to the headplug.

The surgery is similar to that of the wired implant (described in section 2.4.5), but there are some slight differences. The array is passed through the spinal column in the same manner, but due to the size of the implant and location of the entry point at the L4 vertebrae, the electronics package is placed over the spinous process that is used to fix the implant. This slightly alters the process by which the implant is fixed to the spine. After passing a suture through holes in the array daughterboard and the hole in the spinous process, it must then go around the top of the implant and tie it down. The final difference is that the EMG wires no longer originate from the headplug, and instead originate from the implant package.

3.3.2 Multiplexed implant

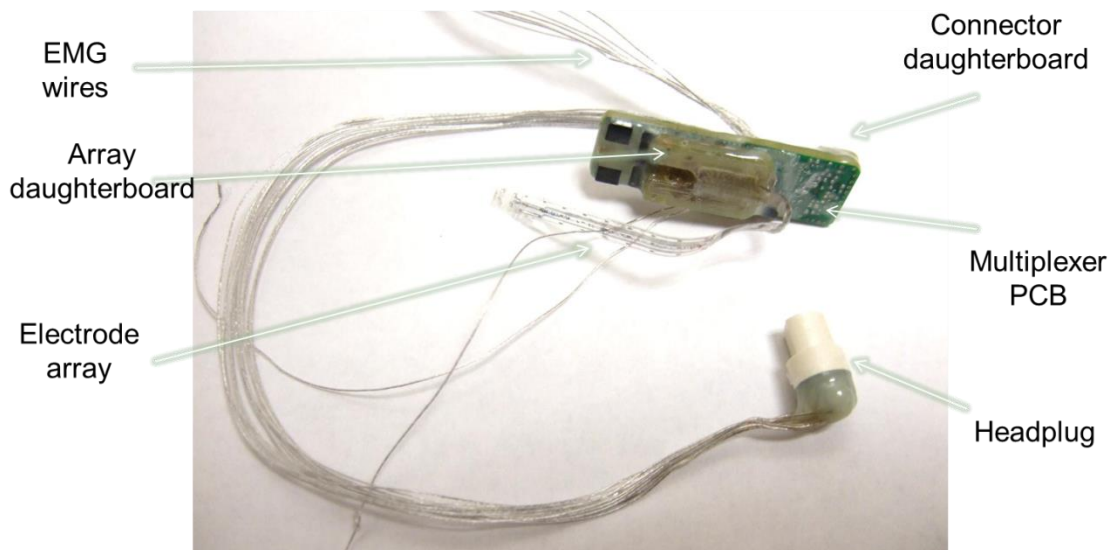


Figure 3.3: Photograph of the multiplexed implant

The finished multiplexed implant can be found in figure 3.3. Due to the reduction in the number of wires from this design, the custom 48-pin headplug is no longer needed, and an Omnetics 12-pin connector is used instead.

3.3.3 Multiplexer Circuit

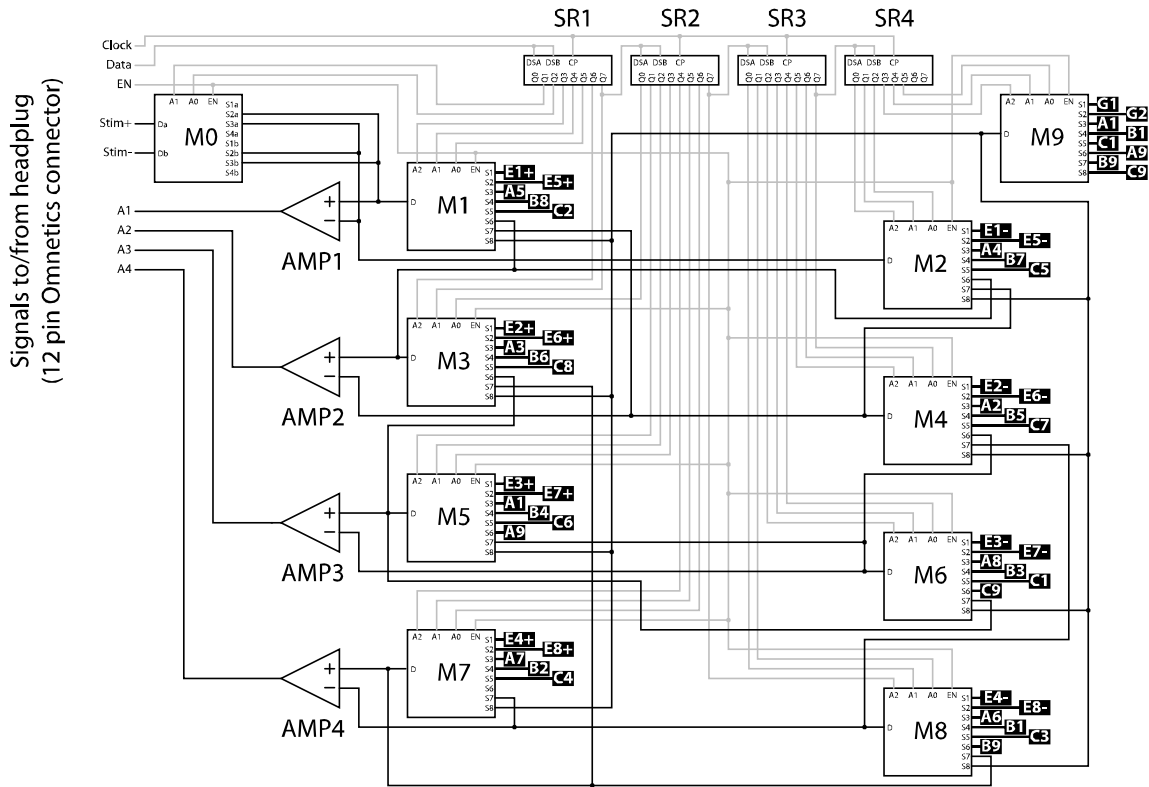


Figure 3.4a: Multiplexer circuit schematic

The schematic of the multiplexer circuit can be found in figure 3.4a. Each black tag in the diagram refers to a connection to a spinal electrode (e.g. “A3” refers to the electrode in column A and row 3), EMG wire (e.g. E5+ and E5- refer to the fifth pair of wires), or ground wire. The four chips labeled SR1 to SR4 are 8-bit shift registers (NXP Semiconductors 74HC164) that are daisy-chained together. Chip M0 is a 2x(4:1) analog multiplexer chip (ADG1209), and chips M1-M9 are 8:1 analog multiplexer chips. Amp1 to Amp4 are differential instrumentation amplifiers (AD8224), and set to a gain of 200. The chips used were chosen to achieve a balance of minimal footprint, low power consumption, and optimal recording characteristics.

There are twelve wires connected to the circuit from the headplug. Three of them (not shown in figure 3.4a) are for power, including V_{dd} (usually 12V, but can be boosted to over 20V), V_{cc} (5V, but can be as low as 2V), and ground. Three are for digital signals to configure the multiplexer: Clock, Data, and EN. The remaining four signals are A1 to A4, which are the output from the amplifiers.

3.3.3.1 Multiplexer Circuit Operation

The desired configuration is achieved by sending a 30-bit serial data stream through Clock and Data (Fig. 3.4a) that feeds into the shift registers SR1 to SR4. The parallel output of these shift registers configures the ten analog multiplexer chips, and the EN signal can enable or disable them as necessary. M0 is used to either disconnect the stimulation wires (Stim+ and Stim-) during recording or choose the polarity during stimulation, while M1 to M9 are interconnected in a way to route to almost any pair of spinal electrodes or EMG wires to either the inputs of AMP1 for recording or the Da and Db terminals of M0 for stimulation. Figure 3.4b shows a sample configuration when the multiplexer is given configuration code 1360505000 (octal representation, where each digit represents 3 bits) to address electrode combination B8-C9. Multiplexer M0 is connected to M1 and M2, but while M1 is directly connected to electrode B8, M2 is not connected to C9, and is thus directed by the circuit to M4 and M6 to address C9. Every possible except when two electrodes are on the same multiplexer, but due to multiplexer M9 providing a second connection to electrodes A1, B1, C1, A9, B9, and C9, such cases are very limited.

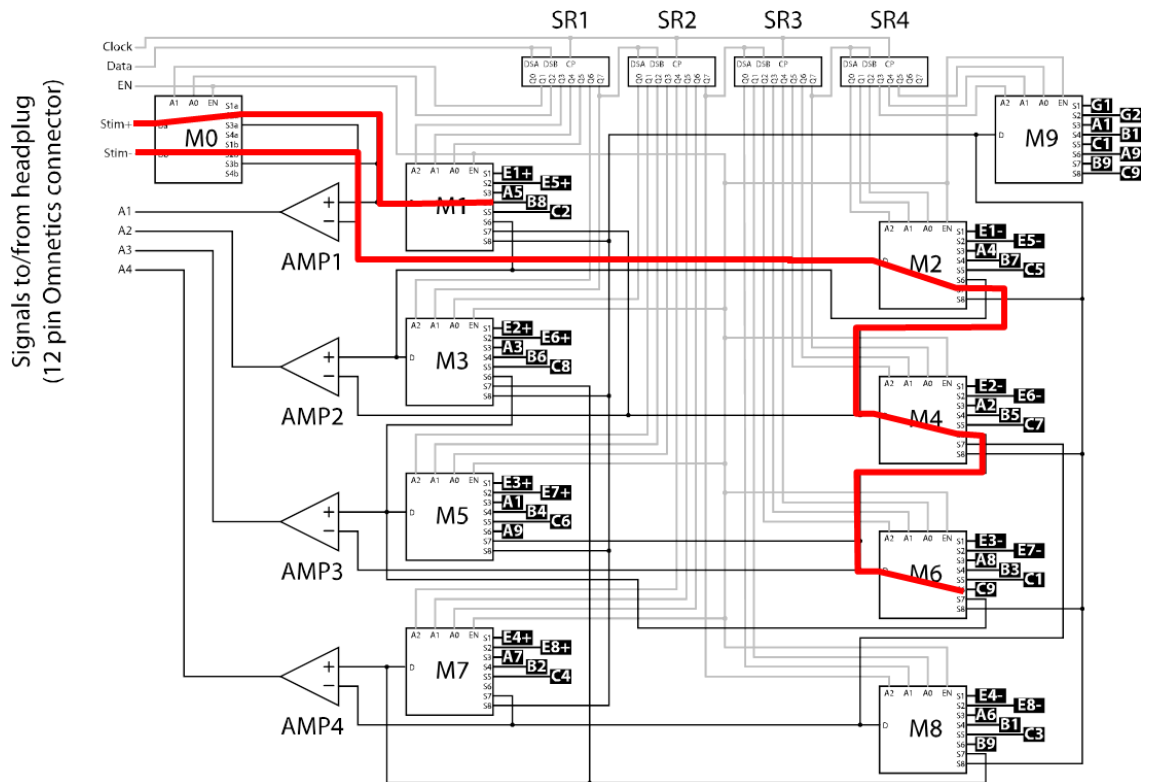


Figure 3.4b: Sample configuration of multiplexer to stimulate combination B8-C9

3.3.3.2 PCB Layout

The circuit board was implemented using four copper layers and measures 10.3 mm by 33.2 mm. To prepare for the long term goal of creating a wireless implant, preliminary components for wireless capability, including a wireless MCU/transceiver reference circuit (Texas Instruments CC1110F32) and wireless power circuit, were also included. Autoroute software (Altium Designer 08) proved to be incapable of placing all traces for this final circuit, even with twice the board area and eight layers, so it was manually routed as shown in figure 3.5. The realized circuit before encapsulation is shown in figure 3.6, with space reserved for wireless components.

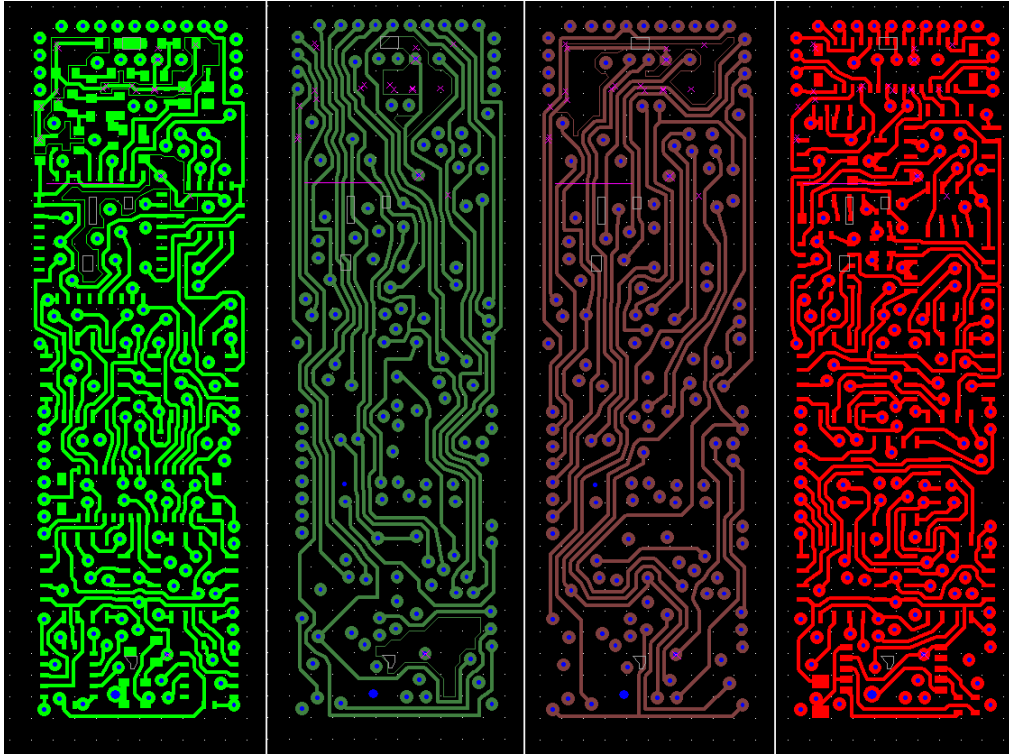


Figure 3.5: Manually routed high-density PCB design for the multiplexer circuit

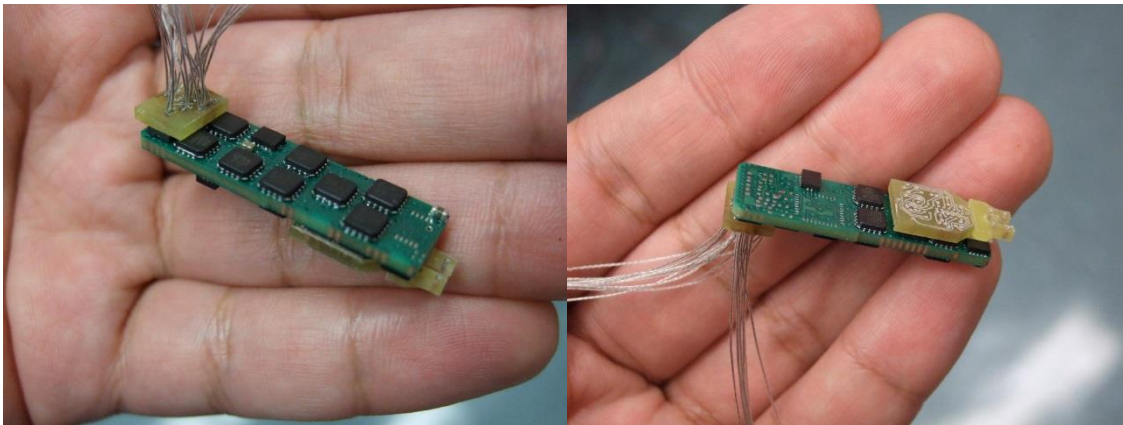


Figure 3.6: The final PCB for the multiplexed implant

3.3.4 Packaging

Correct operation of the multiplexer circuit in vivo is dependent on an adequate sealing procedure. Since the EMG signals can be as small as 0.1mV in amplitude, and the

amplifiers have an input impedances of $10^{13}\Omega$, even miniscule amounts of body fluid leaking onto the PCB can cause significant current to leak into the amplifier inputs from other traces.

The procedure found to work best was a multilayer encapsulation of silicone, parylene-C, and biomedical epoxy. The first sealing layer is 20 μm of parylene-C, but some parts need to be sealed from the conformal nature of the coating. The wires, headplug, and pads on the array daughterboard are protected with polyester tape (3M 8402) and a low temperature water-soluble wax at the ends of the tape. Next, the assembled PCB is dipped in an adhesion promoter solution (100:100:1 ratio of deionized water, isopropyl alcohol, and A-174 adhesion promoter respectively), and then the parylene-C deposition can commence. After removing the tape and wax, a coating of biocompatible silicone (MDX 4-4210) is then applied, using a vacuum chamber to extract as much trapped air as possible before the silicone begins curing. A coating of biocompatible epoxy (Loctite M-121HP) is then applied to add rigidity to the outside, as silicone has a very low Young's modulus and can easily be deformed while inside the animal, which can transmit mechanical forces to encapsulation interfaces.

The microelectrode array is attached at this point, as doing so earlier would risk damaging it. It is coated with a thin layer of silicone as described in section 2.4.2. Finally, a second layer of 20 μm parylene-C is applied, with the microelectrode array, wires, and headplug protected as before with tape and wax. After the deposition, the tape and wax are carefully removed to avoid damaging any of the wires or the electrode array.

3.3.5 Control Box

The control box has an op-amp circuit (figure 3.7) to generate the stimulation signal. The PWM signal is passed through an RC filter and creates any required analog signal at V_{in} (0-2.5 V, $\sim 5 \mu s$ effective pulse rise time). When Mode is low, the op-amp circuit is transformed to that of a positive gain voltage amplifier, otherwise it becomes a voltage controlled current amplifier. When Mode is high, the drain of transistor Q2 is grounded while the drain of Q3 becomes high impedance, transforming the op-amp circuit to that of a current amplifier. This circuit generates the Stim+ signal to be fed into the implant's multiplexer circuit along with the control signals and power lines. The Stim+ signal also is fed back to the NI ADC for voltage monitoring, along with the CurrSense+ and CurrSense- signals for current monitoring. The preamp signals A1-A4 from the implant pass through a voltage divider (adjustable) and then are output to the EMG amplifier (AM Systems Model 1700). The Multiplexer circuit routes the stimulation signals (Stim +ve and Stim -ve) to the chosen electrodes and EMG wires and also routes the chosen electrodes and EMG wires to the 4 available amplifiers.

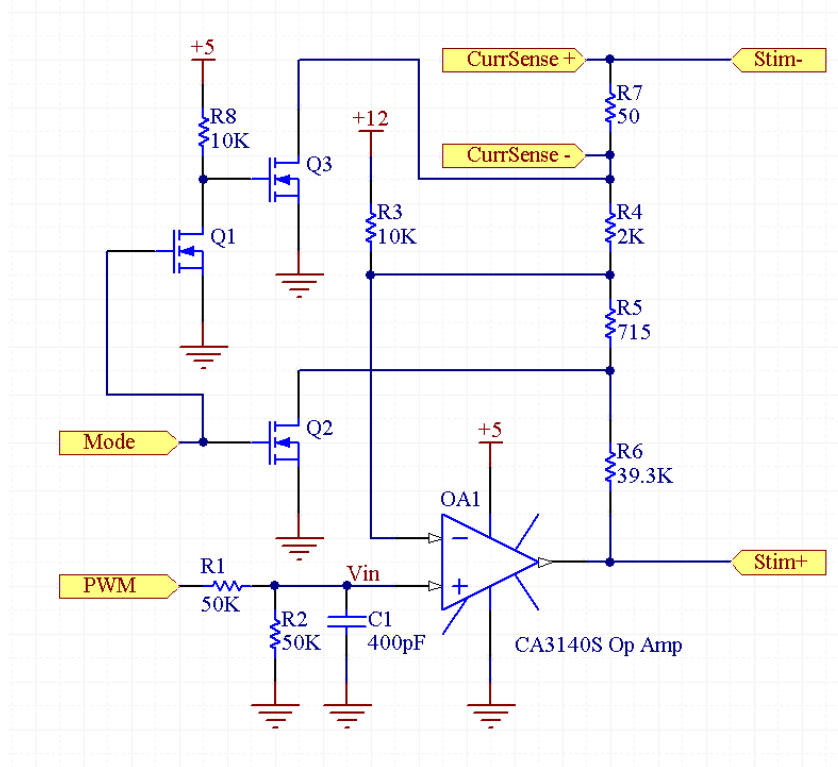


Figure 3.7: Stimulator circuit

3.3.6 Software

To allow the experimenter to control the multiplexed implant, a software interface was developed, as shown in figure 3.8. On the top left, the user can choose which site on the microelectrode array will be the positive electrode and which will be the negative electrode. Certain combinations will be greyed out, because the two electrodes must be on different multiplexers (e.g. A5-B8 cannot be chosen). The software also allows a second pulse to be sent immediately after the first with a different electrode choice. The bottom left specifies what will be recorded, though in general only the EMG channels were recorded. The middle right of the interface allows the user to control the stimulator by specifying the intensity (specified by either pulse voltage or current), pulse duration, and pulse frequency. The top right of the interface monitors both the voltage and current

of the stimulator, and the bottom right monitors the A1-A4 channels of the multiplexer circuit, which are the outputs of the amplifier chips.

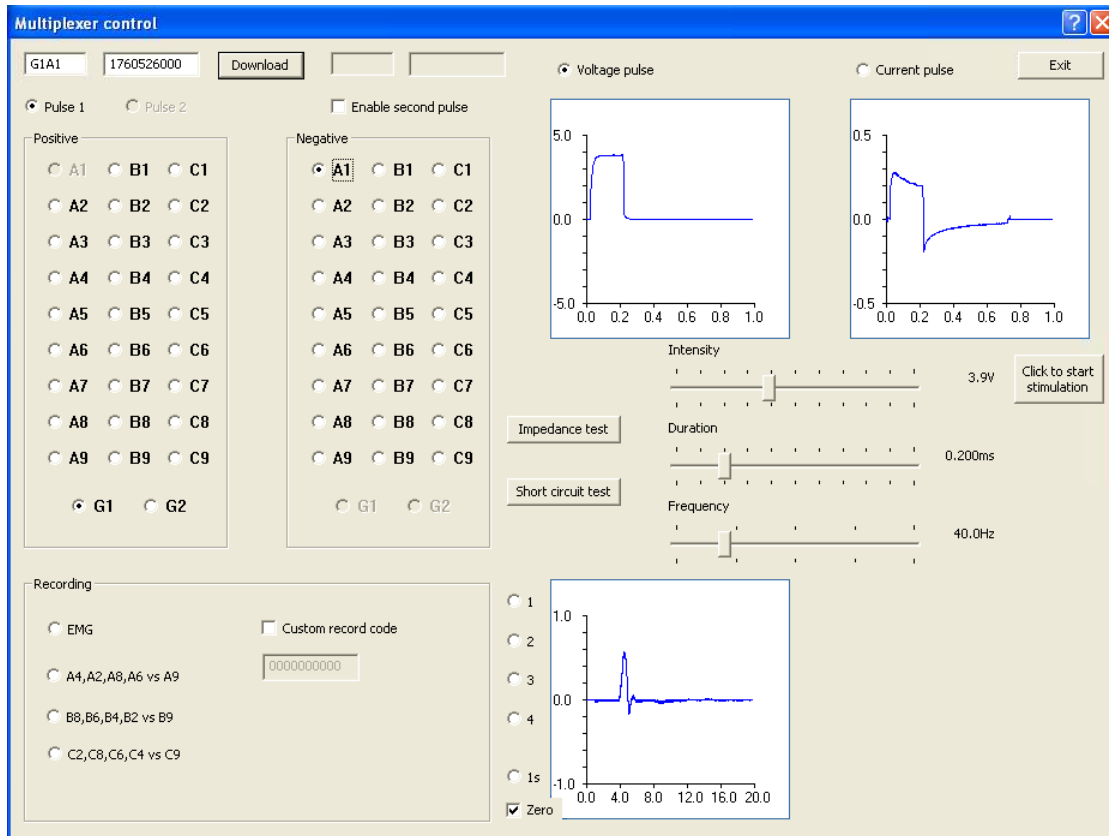


Figure 3.8: Screenshot of software interface during operation

The software was written in C++ and developed using Microsoft Visual Studio 2005, and to interface with the ADC/DIO card (National Instruments PXI-6123), the NI DAQmx library was used. The ADC channels were configured to all record at 50kHz, with two channels used for stimulator monitoring (voltage and current) and four for recording the multiplexer's amplifier output. For output signals, the software calculates and generates a 5 MHz signal stream to be output by the DIO channels of the PXI-6123 and fed to the control box. This signal stream consists of the EN, Clock, and Data signals to control the multiplexer circuit in the implant, PWM (pulse-width modulation) and

Mode signals for stimulation, and a Sync signal to synchronize EMG recordings with the timing of the stimulation.

3.4 Results

The multiplexed implant proved robust enough to gather substantial in vivo data. The two types of experiments performed on the rats are the same as those described in section 1.2, namely the study of evoked potentials from low frequency stimulation and stepping experiments from high frequency stimulation. Encapsulation was a major issue in early implants, but later implants remained functional for up to 8 weeks.

3.4.1 Evoked Potentials

Evoked potentials were recorded while stimulating with the ground electrode (placed subcutaneously on the back of the rat) acting as the anode and each of the electrodes on the array as the cathode. To confirm that the multiplexed implant was recording EMG signals correctly, some animals had a second implant with wires directly (i.e. without any multiplexer circuit) going into some muscles which also had wires from the multiplexed implant. These animals allowed a comparison of signals from the multiplexed implant and direct wire recording using an external EMG amplifier, and the results are shown in figure 3.9. Although the signals are not identical, the match is within expectations for two different wire pairs in the same muscle, and the EMG recording from the multiplexer can be considered accurate.

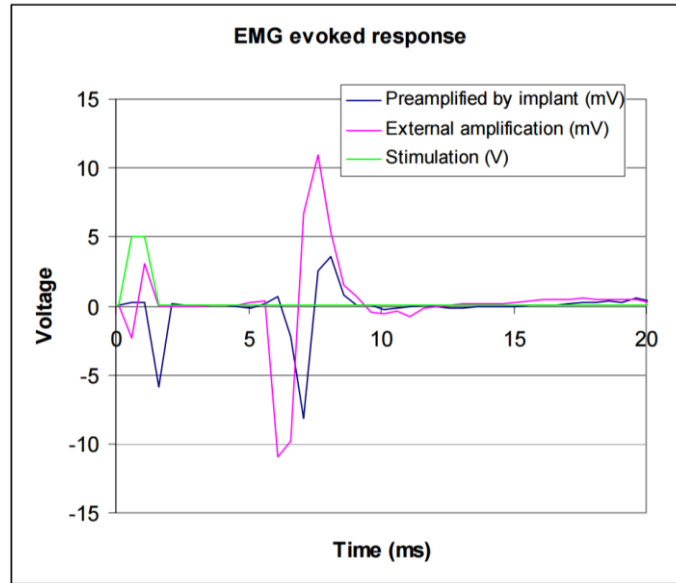


Figure 3.9: Comparison of EMG recordings from the multiplexed implant and direct wire recording with external amplification.

Low frequency (1 Hz) single pulses were applied at 1-8 V in 1 V increments. The responses were divided into 20 ms windows using the stimulation pulse as the trigger. These windows were averaged over 10 evoked responses and the peak response was detected using custom MATLAB code. These peaks then were binned into ER (1-3 ms latency), MR (4-6 ms latency), and LR (7-10 ms). Detailed results for the amplitudes and latencies of the ER, MR, and LR for both the MG muscle (medial gastrocnemius) and TA muscle (tibialis anterior) at different intensities of stimulation can be found in [51]. A sample of the data for the middle response is shown in figure 3.10. In each graph, the bar height represents the magnitude of early response in mW, the color indicates the latency, and there is a bar for each of the 27 electrodes.

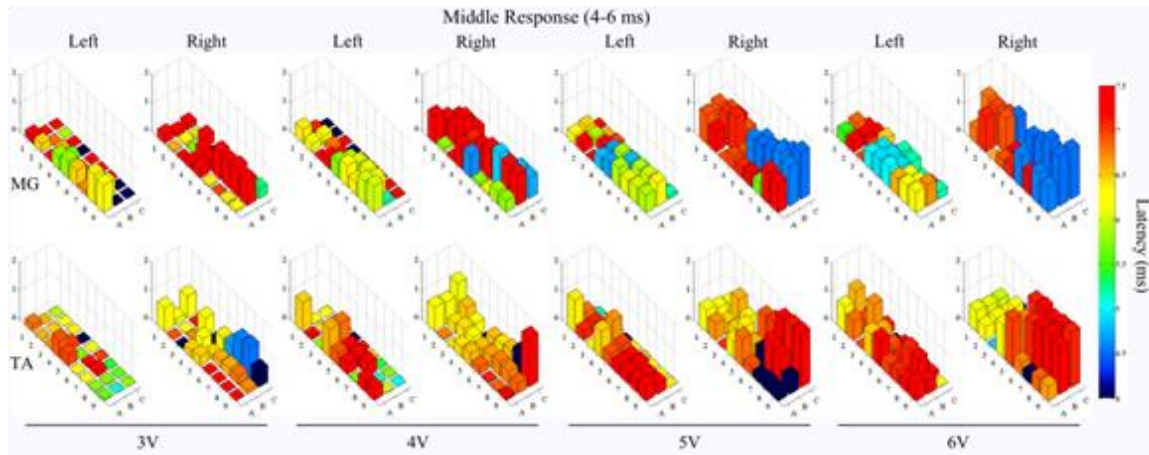


Figure 3.10: Middle response from evoked potentials.

By recording the evoked potentials from specific muscles during monopolar stimulation at different intensities, one can assess the activation of the motor pools of the ankle flexor and extensors in the spinal cord, as shown previously [23-26]. One key observation is that stimulation one side of spinal cord (i.e. columns A or C) generate most activity on the same side of the body (i.e. the left or right hindlimb muscles). This demonstrates the ability to selectively activate different circuitries and to stimulate specific anatomical areas and combinations of motor pools. This potential to selectively activate specific combinations of motor pools and levels of inhibition and excitation translates into the unique capability of electrode arrays to control motor behavior.

3.4.2 Stepping

As before (see figure 2.19), the rat was suspended in a jacket with weight support over a treadmill running at 13.5 cm/s. Different frequencies were tested to facilitate standing and stepping. Stimulation at low frequencies (10-15 Hz) produced vibratory movements in both hindlimbs, but did not facilitate standing or stepping. Stimulation at

higher frequencies (80-100 Hz) at some of the rostral electrode pairs resulted in over-activation of the neuronal circuits and produced some non-specific movements in both hindlimbs with no interlimb coordination. In contrast, stimulation between 40-60 Hz at the rostral electrodes resulted in coordinated activation of flexor and extensor muscles in both hindlimbs leading to partial weight-bearing standing and stepping. Thus, distinct motor responses were induced by stimulation of the rostral electrodes at different frequencies.

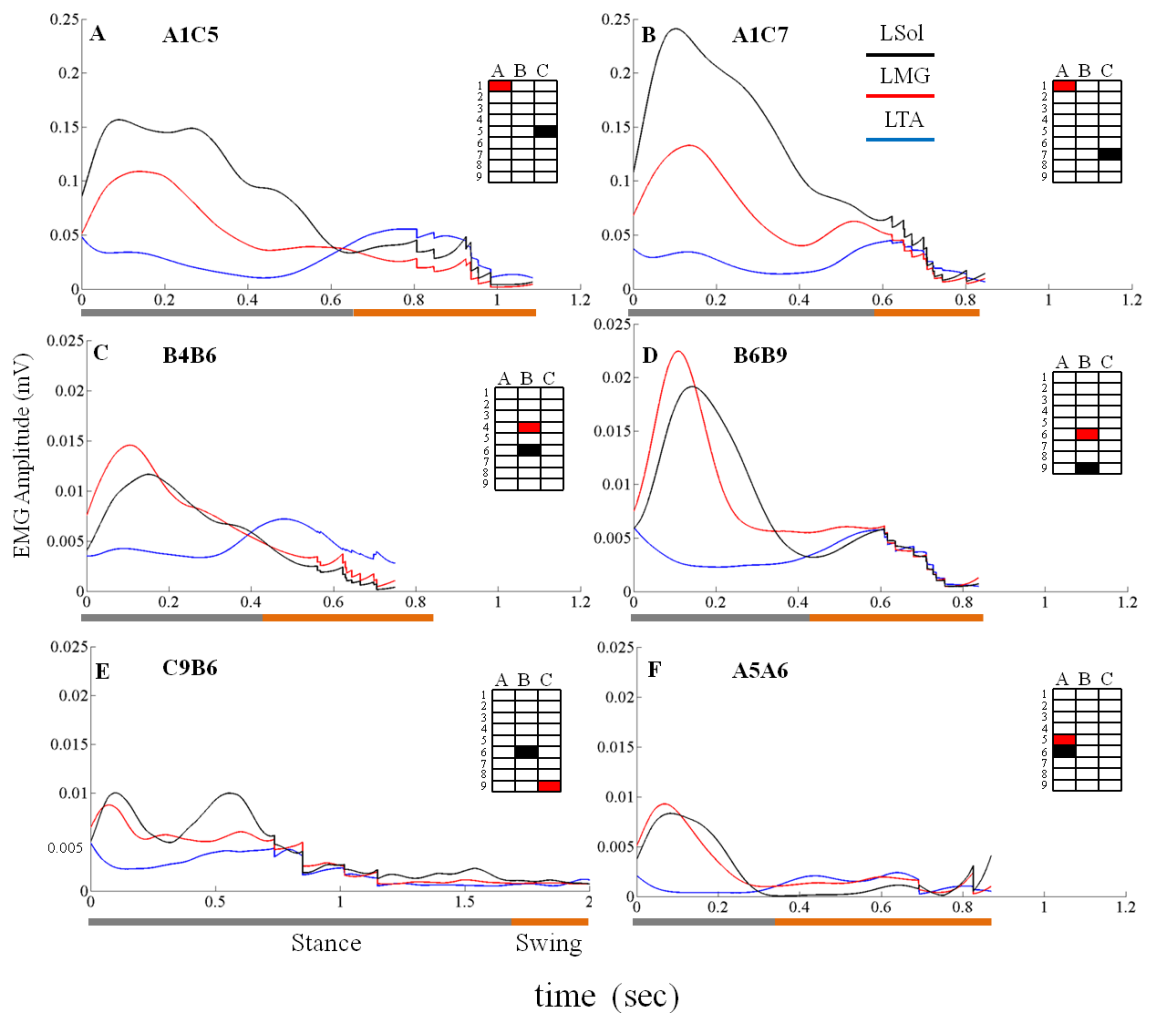


Figure 3.11: Stepping responses with different combinations

Bipolar stimulation (40 Hz, pulse width of 0.2 ms, and 3-4 V) using different pairs of electrodes on the spinal cord showed different stepping patterns. The results using 6 different bipolar combinations are shown in figure 3.11. These graphs don't show direct EMG signals, but rather the amplitude of their envelope over the course of the stride [52]. Four combinations with the cathode rostral to the anode resulted in coordinated bilateral stepping showing good interlimb coordination, with two providing good body support (combinations A1-C5 and A1-C7) and two others providing lower body weight support (combinations B4-B6 and B6-B9). Combination C9-B6 produced poor stepping, and with combination A5-A6 the rat was able to generate step-like movements, but with little or no body weight support.

3.5 Summary

A multiplexed microelectrode implant system for spinal cord stimulation was designed, built, and successfully implanted. As compared to the wired implant, the multiplexed implant reduced the number of wires passing down the rats neck to 12 while still being able to address 45 different locations: 27 microelectrodes, 2 ground wires, and 16 EMG wires (although only 8 EMG wires were implemented). It contains a multiplexer circuit that routes an external stimulator signal to almost any pair of electrodes and also routes signals to amplifiers for recording functionality. An encapsulation process was developed to protect the circuit from body fluid, and was achieved using the low cost materials of silicone, parylene-C and epoxy. The process protected the circuit enough to remain functional for up to 8 weeks. Software and external electronics were developed to easily control the implant. To our knowledge, this is the first

In vivo testing proved that the implant was able to epidurally stimulate the spinal cord, and unlike the wired implant, the 12 wires to the headplug was low enough to avoid any harm to the animal. As with the implant described in the previous chapter, stepping was achieved 8-10 days after transection, which is much sooner than previous wire based studies. Detailed data was obtained showing that the multiplexed microelectrode array implant allows high spatial resolution for stimulation and the ability to selectively activate different neural pathways within the spinal cord. This not only allows for better tuning of stimulation to facilitate standing and stepping in adult spinal rats, but it also provides the capability to evoke motor potentials and thus a means for assessing connectivity between sensory circuits and specific motor pools and muscles. The data underscores the importance of electrode location and stimulation properties for future therapeutic devices to maximize motor function restoration after SCI.

4. Wireless Multielectrode Array Implant

4.1 Introduction

Biocompatibility of implants is a crucial factor in successfully collecting data in chronic experiments. For microelectrode array implants, as the number of electrodes increases, so do the required connections to a wire bundle in order to make connections with external electronics, and the probability of success of the implant due to potential tissue damage and infections caused by the wire bundles. The work in the previous chapter partially addressed this problem by employing a multiplexer to reduce the number of required connections, but it is desirable to eliminate the wired connections entirely and develop a fully wireless implant with multi-channel stimulating/recording. Such a technology is particularly important for scaling up this spinal cord stimulator to different species, such as cats, monkeys, or humans, as biocompatibility is of greater importance. Eliminating wires and the headplug also make the device more easily implantable, so fewer changes are needed to adapt the device to different purposes, locations on the body, and animals.

A key component of any fully wireless implant system is wireless power transfer. In the early days of electromagnetism, wireless power transfer was most famously pursued by Nikola Tesla [53]. The allure of wireless power transmission for convenience is obvious, but the strongest need for technology likely exists in the biomedical device industry, where wireless power has a long history [54,55] through its most common form: the near-field inductively coupled link. Although newer developments have demonstrated high coupling efficiency at middle distances [56], it requires very precise tuning to match

the ultra-high Q of self-resonant coils. The work presented here will also use inductive coupling to implement wireless power transfer.

4.2 Design Requirements

The basic design requirements for the wireless implant do not change from those introduced in section 3.2, but additional parameters will need to be considered now that the implant will be completely wireless and can't use external components.

There must be a MCU (microcontroller unit) and wireless transceiver in the device to control the device, receive stimulation parameters, and transmit recorded waveforms. Fortunately, there are a number of combined MCU/transceiver SoCs commercially available. A sampling rate of 2kHz is the minimum needed to capture most of the relevant biological data, and for four recording channels at 8 bits per sample, that suggests 64 kbps required data transmission. While the MCUs are theoretically capable 500 kbps, preliminary research suggested that real world data transfer was usually under 100 kbps. That suggest the radio will be on most of the time. A quick survey revealed that the radio alone on all suitably sized SoCs needs ~50mW of power (~20-mA at a V_{cc} of around 2-3V) whether receiving or transmitting.

From this, the specifications of the wireless power subsystem can be determined. The multiplexer circuit consumes minimal power aside from the amplifiers, which consume a minimum of roughly 4mW each, but to make sure there was enough margin of error, it was assumed that the circuit would need up to 100mW of wireless power delivered. A battery was considered, but at that power requirement, only a few minutes of operation could be achieved given the minimal room in the implant. The wireless power

subsystem would also have to deal with considerable movement of the mouse during stimulation, so a target maximum separation goal of 5cm was set.

4.3 Wireless Power Theory

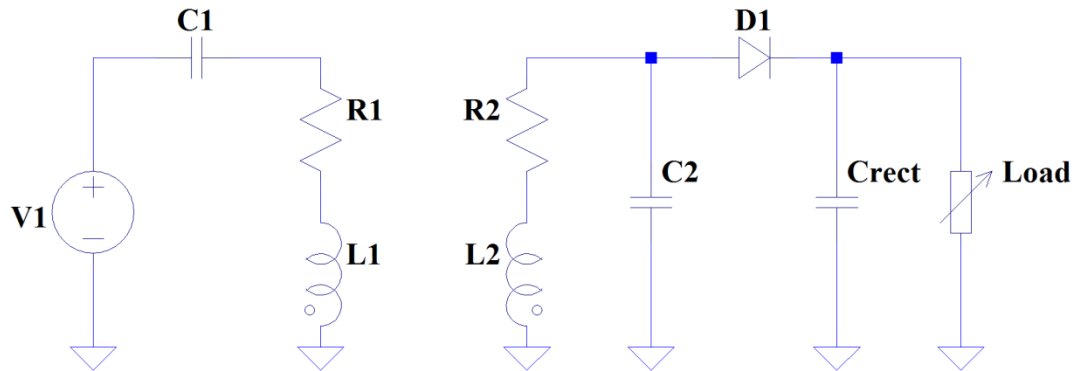


Figure 4.1: Simplified circuit for inductive power transfer

The simplified circuit for wireless power transfer using an inductive link is shown in figure 4.1. The left side shows the primary circuit, composed of an AC voltage source powering the a primary coil and its RLC circuit, while the right side shows the secondary coil and its RLC circuit, with the induced voltage being rectified by a diode to power a DC load. Both RLC circuits are tuned to the same resonant frequency. To develop an analytical model for wireless power transfer, it is helpful to use a linear approximation.

4.3.1 Linear Model Approximation

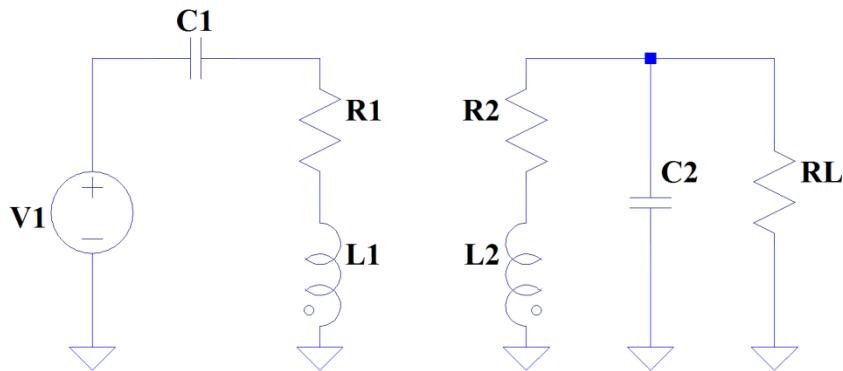


Figure 4.2. Linear model for inductive power transfer

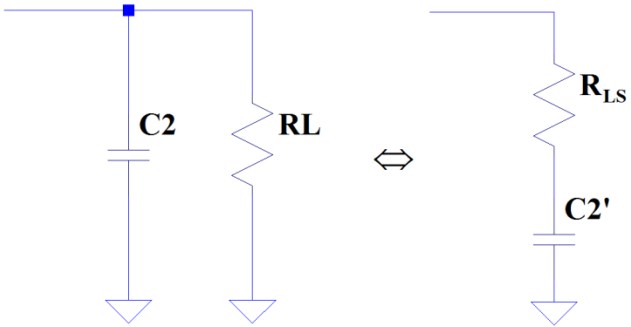
Inductive power transfer between two coils can be approximated and analyzed through the use of an AC linear model, as seen in Figure 4.2. Here, the primary circuit is on the left, with the primary coil being represented by L1 and its parasitic resistance R1, and the secondary circuit is on the right, with secondary coil L2 and its parasitic resistance R2. C1 and C2 are capacitors chosen to be resonant with the coils. The load of the electronics is approximated by a resistor R_L with equal power consumption:

$$P_{L,DC} \equiv P_{L,AC} = \frac{V_{AC}^2}{2R_L}$$

$$\Rightarrow R_L = \frac{V_{AC}^2}{2P_{L,DC}}$$

Since the actual circuit (Figure 4.1) has a non-linear element (the diode), there is no strictly sinusoidal V_{AC} . However, the voltage across the secondary coil is still a distorted sinusoid whose amplitude is roughly equal to V_{DC} (the rectified voltage on C_{rect}) plus the voltage drop of the rectifier (typically 0.3V for a Schottky diode). For example, a wireless implant electronics load consuming 100mW at 5V would have an

equivalent R_L of 140Ω . We can further transform R_L in to an equivalent resistance R_{LS} that appears in series with R_2 :



$$\begin{aligned}
 Z_p &= \frac{1}{j\omega C_2 + \frac{1}{R_L}} = \frac{R_L}{j\omega C_2 R_L + 1} = \frac{R_L(1 - j\omega C_2 R_L)}{1 + (\omega C_2 R_L)^2} \\
 &= \frac{R_L}{1 + (\omega C_2 R_L)^2} + \frac{1}{j\omega C_2} \left[\frac{(\omega C_2 R_L)^2}{1 + (\omega C_2 R_L)^2} \right] \\
 \therefore R_{LS} &= \frac{R_L}{1 + (\omega C_2 R_L)^2}, \quad C_2' = C_2 \left[1 + \frac{1}{1 + (\omega C_2 R_L)^2} \right]
 \end{aligned}$$

Figure 4.3: Impedance transformation of the parallel load R_L into a series load R_{LS}

4.3.2 Wireless Power Efficiency Derivation

Applying Kirchoff's Voltage Law to the circuit of figure 4.2, and noting that the mutual inductance between the coils is $M = k\sqrt{L_1 L_2}$ (k is the coupling coefficient determined by the size and separation of the coils), we obtain the following system of equations in the AC domain:

$$V_1 = \left(\frac{1}{j\omega C_1} + R_1 + j\omega L_1 \right) I_1 + j\omega M I_2$$

$$0 = \left(\frac{1}{j\omega C_2} + R_2 + R_{LS} + j\omega L_2 \right) I_2 + j\omega M I_1$$

We can choose C_1 and C_2 such that $\frac{1}{j\omega C_1} + j\omega L_1 = 0$ and $\frac{1}{j\omega C_2} + j\omega L_2 = 0$, so

that the primary and secondary circuits resonate at the same frequency, and the solution to the system of equations is then simply:

$$V_1 = I_1 \left(R_1 + \frac{\omega^2 M^2}{R_2 + R_{LS}} \right)$$

$$= I_1 (R_1 + R_{refl}), \quad R_{refl} \equiv \frac{\omega^2 M^2}{R_2 + R_{LS}}$$

It is therefore apparent that the secondary circuit effectively appears in the primary circuit as a reflected impedance R_{refl} in series with R_1 . The power supplied by V_1 is therefore divided between R_1 (primary coil parasitic resistance) and R_{refl} (secondary circuit total load) as a simple series voltage divider; furthermore, the power delivered to R_{refl} is similarly divided between resistances R_2 (secondary coil parasitic resistance) and R_{LS} (the load of the electronics in the wireless implant) in series. Recognizing this, we can express the efficiency of the wireless power transfer as a simple product of two voltage dividers:

$$\eta = \frac{R_{refl}}{R_1 + R_{refl}} \cdot \frac{R_{LS}}{R_2 + R_{LS}}$$

We can also simplify this equation with various dimensionless parameters. The coils and their parasitic resistances can be described by defining the quality factors

$Q_1 \equiv \frac{\omega L_1}{R_1}$ and $Q_2 \equiv \frac{\omega L_2}{R_2}$, the load R_{LS} can be described as ratio $\beta \equiv \frac{R_{LS}}{R_2}$, and we can

also define a figure of merit $\alpha \equiv k^2 Q_1 Q_2$. The reflected resistance can then be rewritten as follows:

$$\begin{aligned}
 R_{refl} &\equiv \frac{\omega^2 M^2}{R_2 + R_{LS}} \\
 &= \frac{\omega^2 k^2 L_1 L_2}{R_2 (1 + \beta)} \cdot \frac{R_1}{R_1} \\
 &= R_1 k^2 \left(\frac{\omega L_1}{R_1} \right) \left(\frac{\omega L_2}{R_2} \right) \frac{1}{(1 + \beta)} \\
 &= R_1 (k Q_1 Q_2) \frac{1}{(1 + \beta)} \\
 R_{refl} &= R_1 \left(\frac{\alpha}{1 + \beta} \right)
 \end{aligned}$$

Finally, the wireless power transfer efficiency can be rewritten:

$$\begin{aligned}
 \eta &= \left(\frac{R_{refl}}{R_1 + R_{refl}} \right) \left(\frac{R_{LS}}{R_2 + R_{LS}} \right) \\
 &= \left[\frac{R_1 \left(\frac{\alpha}{1 + \beta} \right)}{R_1 + R_1 \left(\frac{\alpha}{1 + \beta} \right)} \right] \left[\frac{\frac{R_{LS}}{R_2}}{\frac{R_2}{R_2} + \frac{R_{LS}}{R_2}} \right] \\
 &= \left(\frac{\frac{\alpha}{1 + \beta}}{1 + \frac{\alpha}{1 + \beta}} \right) \left(\frac{\beta}{1 + \beta} \right) \\
 \eta &= \left(\frac{\alpha}{1 + \alpha + \beta} \right) \left(\frac{\beta}{1 + \beta} \right)
 \end{aligned}$$

4.3.3 Wireless Power Efficiency Optimization

Efficiency is an increasing function of α , but is maximized with an optimal β . It should be noted that α is defined by physical constraints of the system, as there is a limit to how high we can make the quality factor of coils, and the coupling factor k is defined

by requirements of the project. In contrast, β is a design parameter due to the nature of coils. A coil of given size constraints can be given double the number windings if the conductor cross section is halved. This quadruples the inductance, but also quadruples the parasitic resistance (due to doubling the length and halving the cross sectional area), and thus its quality factor Q stays the same. Alternatively, an impedance transformation can be used in the secondary circuit, again retaining the same Q_2 but allowing R_2 and L_2 to change as long as their ratio remains constant. Therefore, given the constraint on Q_2 ,

$\beta \equiv \frac{R_{LS}}{R_2}$ is freely specified by choosing L_2 . The efficiency equation above can be

maximized as a function of β using calculus, and we obtain the following optimal efficiency:

$$\begin{aligned}\eta &= \left(\frac{\alpha}{1 + \alpha + \beta} \right) \left(\frac{\beta}{1 + \beta} \right) \\ \frac{\partial \eta}{\partial \beta} &= \frac{\alpha(1 + \alpha - \beta^2)}{(1 + \alpha + \beta)^2 (1 + \beta)^2} \\ \frac{\partial \eta}{\partial \beta} = 0 &\Rightarrow \beta^2 = 1 + \alpha \\ \therefore \beta_{opt} &= \sqrt{1 + \alpha} \\ \therefore \eta_{opt} &= 1 - \frac{2}{1 + \sqrt{1 + \alpha}}, \quad \alpha^2 \equiv kQ_1Q_2\end{aligned}$$

As a point of reference, if $\alpha=0.5$ (e.g $k=0.01$, $Q_1=100$, $Q_2=50$), then $\eta_{opt} = 10.1\%$.

If α is even smaller, then $\eta_{opt} \approx \alpha/4$. Ignoring losses, a load of 100mW can be supplied with wireless power if the primary circuit can deliver 1W of power into the coil. It should be noted that while these calculations present β_{opt} as a function of α , a single fixed β must be chosen for a wireless power design; otherwise, the coil inductance and resonance capacitor would need to change dynamically. Since α is proportional to k^2 , it will vary

drastically in magnitude with distance as the coupling factor changes. Figure 4.4 shows a plot of efficiency as a function of α . As can be seen, a value of 2 chosen for β is almost optimal at low coupling factors (e.g. for $\alpha=0.5$, $\eta = 9.5\%$) while retaining good coupling efficiency at higher values of α .

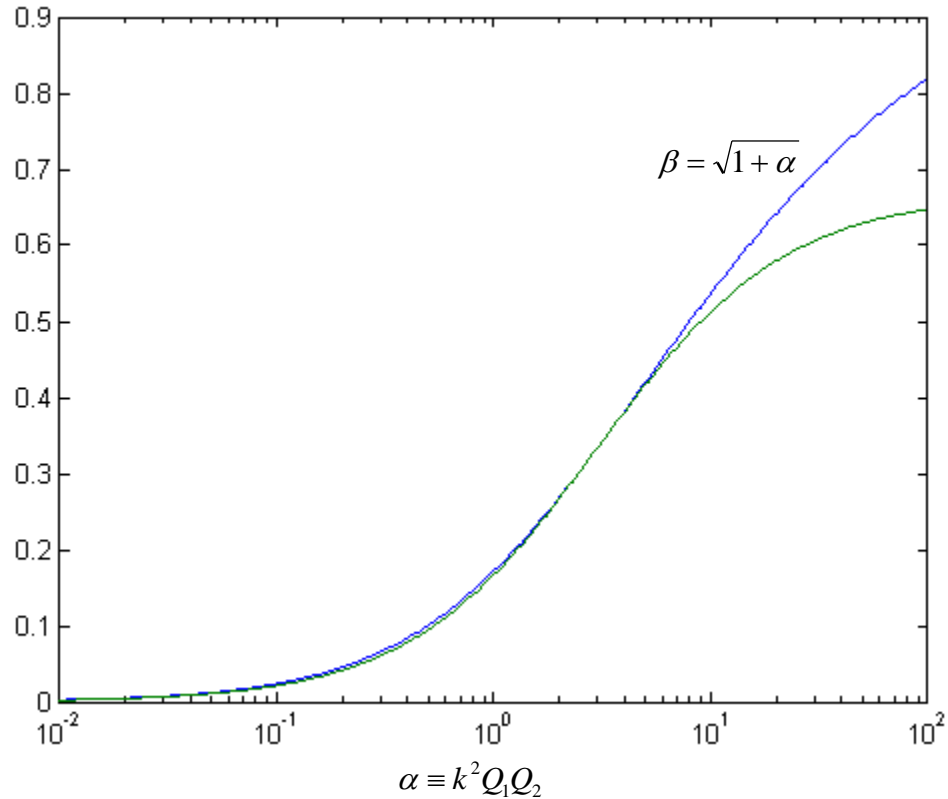


Figure 4.4: A plot of wireless power transfer efficiency.

4.4 Wireless Power Implementation

4.4.1 High Q coils

As noted in section 4.3.2, high Q coils are critical to make α as large as possible to improve coupling efficiency. It was found that the straightforward solution of using thicker wire to reduce coil resistance has serious limitations, as shown in figure 4.5.

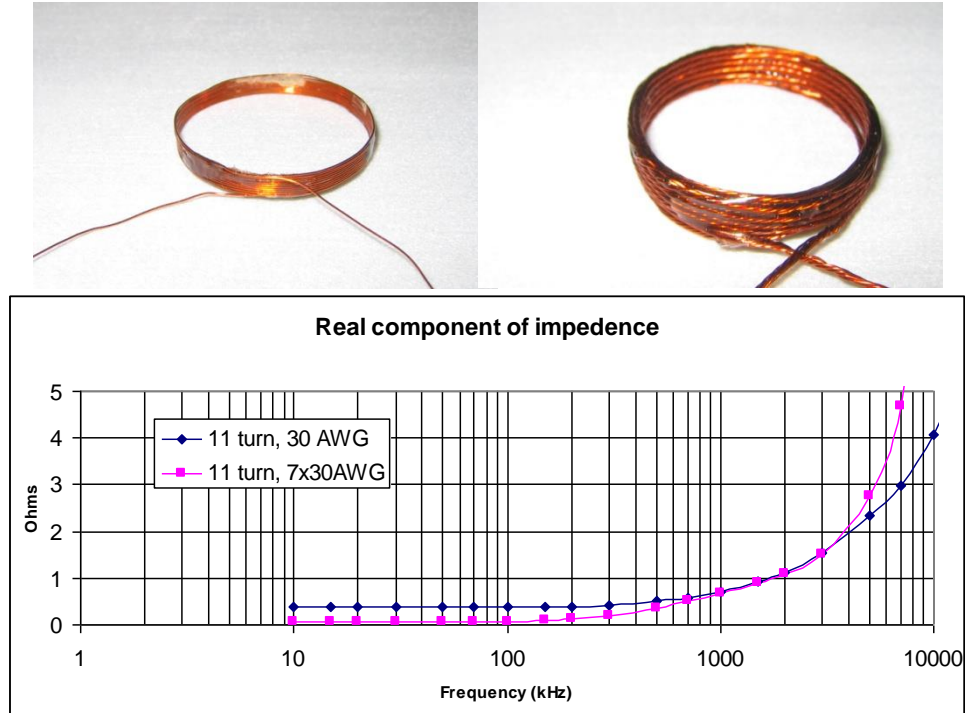


Figure 4.5: Comparison of parasitic resistance between two 11 turn coils

At a frequency of 3 MHz, the use of 7x the copper did not improve parasitic resistance at all, despite achieving the expected resistance reduction at lower frequency. This magnitude of impedance increase cannot be attributable to the skin effect alone, as the skin depth of copper at 3MHz is $38\mu\text{m}$, and the 30 AWG copper wire ($127\mu\text{m}$ radius) should only have increased resistance by a factor of 2x vs DC, whereas the observed increase was 25x. After additional research, the cause was found to be what is known as the “proximity effect”, in which the magnetic field from neighboring currents (as opposed to a wire’s own current alone in the skin effect) cause highly uneven current distribution in the coil windings. A simulation was performed using Comsol 4.2a to better understand the issue. Figure 4.6 illustrates the results of the simulation and a good match

with measured results up to 5 MHz, beyond which it is suspected that parasitic coil capacitance affected impedance measurement.

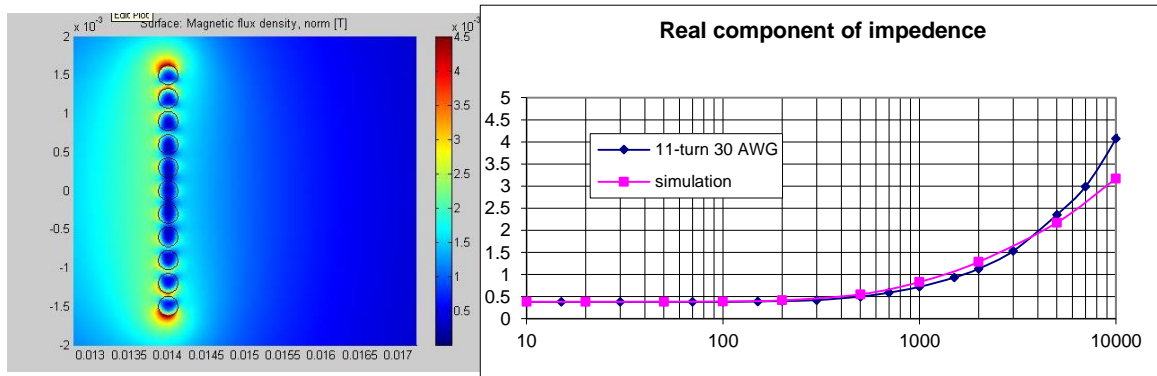


Figure 4.6: Simulation of coil parasitic resistance. Left: Simulated cross sectional view of coil windings showing magnetic flux. Right: Simulation shows agreement with measurements.

To mitigate the proximity effect, litz wire was used. Litz wire is comprised of many fine strands of insulated wire in parallel, twisted in a way that promotes even current distribution among the strands. 30xAWG48 Litz wire was used, as it was the finest readily available wire. Measurement of high Q by impedance analyzers is prone to error, as it requires very accurate phase measurement of the impedance. As an example, if a $Q=100$ coil has its phase measured to $\pm 0.5^\circ$ accuracy, the reading could vary from $Q=53$ to $Q=785$. A better way to measure Q is to solder a high-Q (i.e. $Q>2000$) resonance capacitor in parallel with the coil to create an RLC circuit, and measure the FWHM of the real part of the impedance spectra to determine $Q=\Delta f/f_0$. As a secondary measurement, the peak impedance will be $Z \approx Q^2 R$, and R of the coil can be measured using the same capacitor in series. Using this technique, a peak Q_1 of 170 ± 10 was obtained for the primary coil at 3.2MHz, and $Q_2=80 \pm 5$ for the secondary coil. Q decreases at higher

frequencies due to the proximity effect, and decreases at lower frequencies due to the ω term in $Q = \frac{\omega L}{R}$.

4.4.2 Primary Power Amp

The primary amplifier generates a sinusoidal waveform to power the primary coil. A power target of roughly 1W was found to be practical, as it was sufficient to power 100 mW at 5% wireless coupling efficiency, and higher power would heat up the coil too much. The most efficient way to drive a power coil is with a class E amplifier [57], as during operation it uses a transistor (usually a Power MOSFET) that is either fully on or off, burning substantial power only during the transition time. A class E amplifier was designed, but it was found to require extremely precise tuning, as capacitance changes of only 0.1pF could substantially alter the drive waveform. Since amplifier efficiency was not a major concern at this point, a class C amplifier was used instead. The best amplifier chip found at a reasonable price was the LT1206 current feedback amplifier. It is capable of $\pm 12.5V$ output swing into a 50Ω load (i.e. 250mA), i.e. 1.5W for a sinusoid. A current feedback amplifier was necessary to provide the necessary slew rate of at least $200V/\mu s$ required for a 10V sinusoid at 3.2MHz ($\frac{dV}{dt}_{\max} = 2\pi fA$). Figure 4.7 show the final circuit and the realized amplifier.

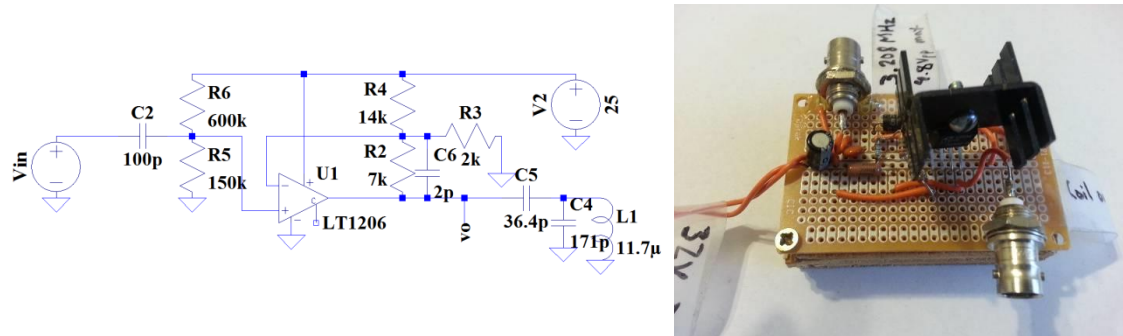


Figure 4.7: Primary amplifier schematic and photograph

It should be noted that the simplified circuit in Fig 4.1 would require an extraordinary drive current into the coil. The coil cannot have an arbitrarily large inductance L_1 or its self-resonant frequency will be too low for operation at 3.2MHz, and if it is also high Q , then $R_1 = \frac{\omega L_1}{Q_1}$ will necessarily be small. The schematic in figure 4.7 also shows an impedance transformation applied to the coil L_1 with capacitors C_4 and C_5 , so that at the amplifier's output (labeled "vo"), the apparent load of the coil is $\sim 45\Omega$ without the load of the secondary circuit and entirely real.

4.4.3 Power Delivery Control

The secondary circuit can apply a drastically changing load to the primary circuit.

Recall that $R_{refl} = R_1 \left(\frac{\alpha}{1 + \beta} \right)$, and that $\alpha \equiv k^2 Q_1 Q_2$, so if k doubles, then reflected load

will quadruple, and power delivered can go up or down, depending on the total load. To deliver a constant amount of power, the power amplifier's voltage must vary, as shown in Figure 4.8. Because the secondary circuit may change its load depending on what the

implant is doing, and the coupling factor can also change, it must communicate to the primary side about whether to increase or decrease power.

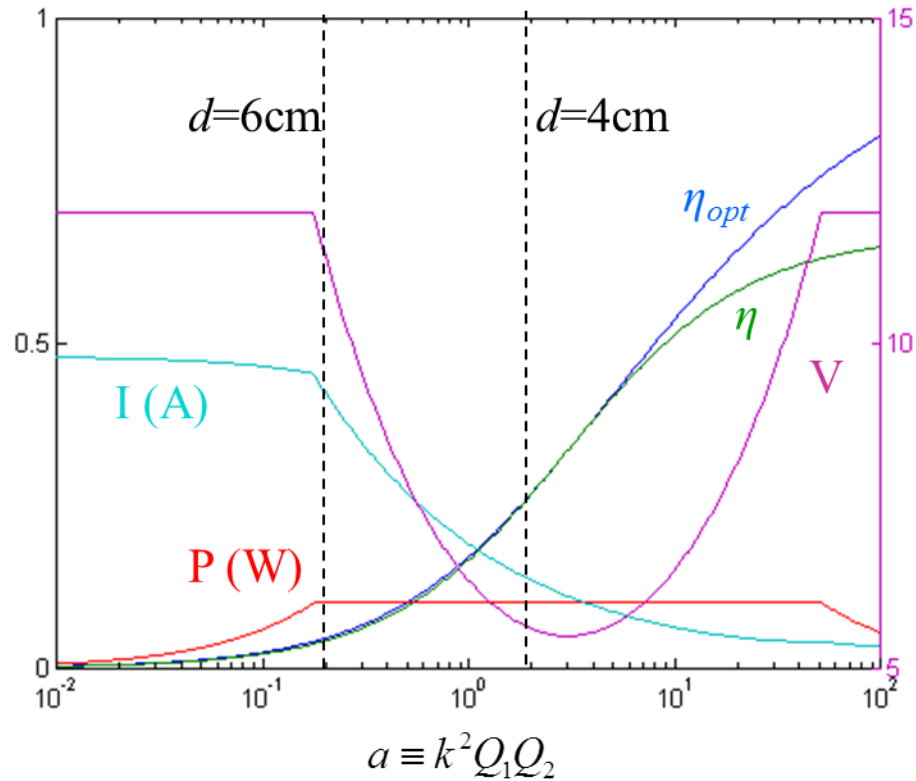


Figure 4.8: Ideal wireless power delivery. As a changes, the primary amplifier's voltage (purple, right scale) must adjust to deliver 100mW power (red, left scale). The current (cyan, left scale) will also change as a result of the reflected secondary load changing in impedance. Two distance markings are labeled.

However, it was found that software communication was not quite robust enough for the most extreme changes in power delivery. During testing, it was eventually found that after a sudden movement, a chip failure occurred, despite the presence of Zener diodes for protection. To prevent this from happening again, a subcircuit was designed for the implant to short circuit its RLC resonator if too much power is delivered, effectively disabling the absorption of power from the primary circuit.

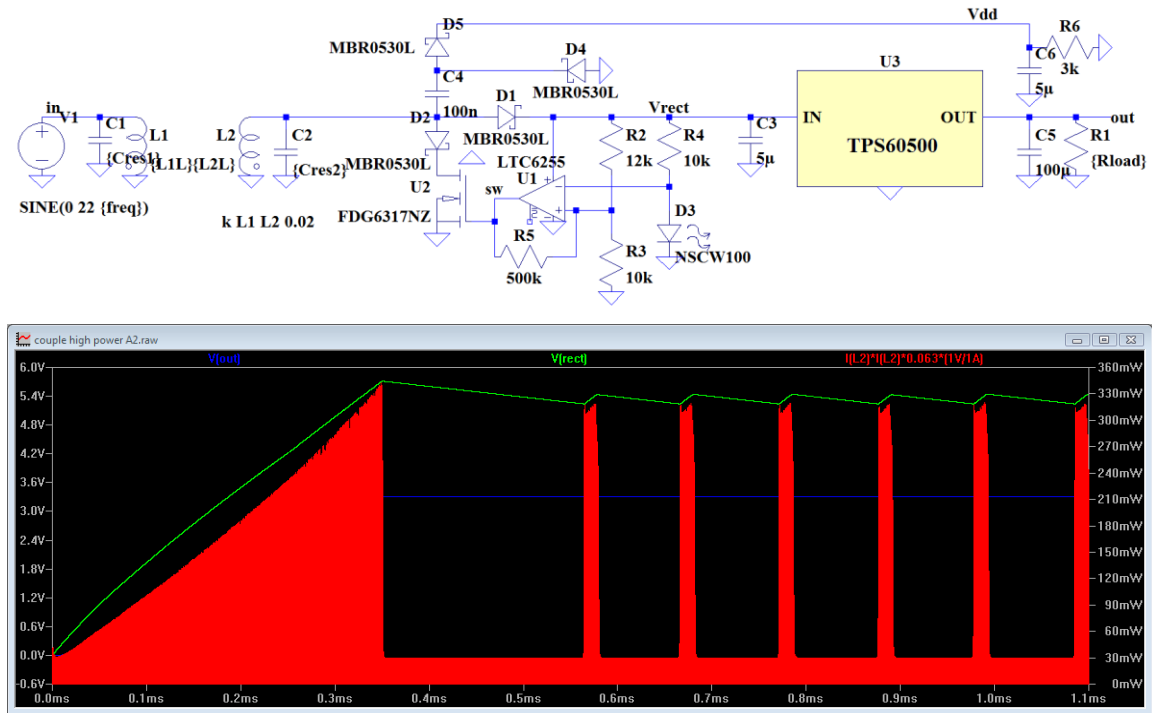


Figure 4.9: Circuit to regulate power absorption by the secondary coil and simulation results. The green trace is the rectified voltage (left scale), and the red trace shows instantaneous power dissipation by the coil (right scale).

Figure 4.9 illustrates the circuit schematic and simulation results. MOSFET U2 and diode D2 are placed across the coil L2. The gate of the MOSFET is connected to op amp U1, which is configured as a comparator circuit with hysteresis. The output of a voltage divider is connected to the positive and negative inputs of op amp U1, with the latter divider using diode D3 to serve as a reference voltage. If the rectified voltage (the node labeled “Vrect”) at C3 is too low, then the positive input of U1 will be low enough to saturate the op amp output at 0V. This turns off MOSFET U2, and allows wireless power to be delivered as usual. Note that R5 provides positive feedback to the op amp U1. The rectified voltage must then rise to 5.4V before the comparator swings to positive saturation. At that point, the comparator turns transistor U2 on, and L2 is unable to resonate with the MOSFET short circuiting it. Moreover, the feedback from R5 now

requires the rectified voltage to drop down to 5.1V before U1 swings low again. The simulation waveforms in Figure 4.9 verify this behavior. The red waveform is instantaneous power dissipation of coil L2, and thus has a carrier frequency of 3.2MHz (which is too high a frequency for the time scale of the graph, and why the waveform appears solid red). Its average over a few μs will be half of the peak seen in the figure. When such a simulation was performed without this power absorption regulation subcircuit, and with identical primary side voltage, the ramping of power absorption seen in Figure 4.9 would continue until it averaged 656mW. With the subcircuit present, it averages at most 160 mW, and only 15mW turning off when not needed.

After the coil's power absorption is controlled, the implant requires 12V (Vdd) and 2.4V (Vcc) power rails. A voltage multiplier (seen at the top of Figure 4.9 with components D4, D5, and C4) provides Vcc, and it is regulated with a LM3840-12 linear regulator. The rectified voltage of 5.1-5.4V is converted to Vcc using a Texas Instruments TPS60500 charge pump regulator, which is much more efficient than a linear regulator for such a large voltage difference.

4.5 Wireless implant

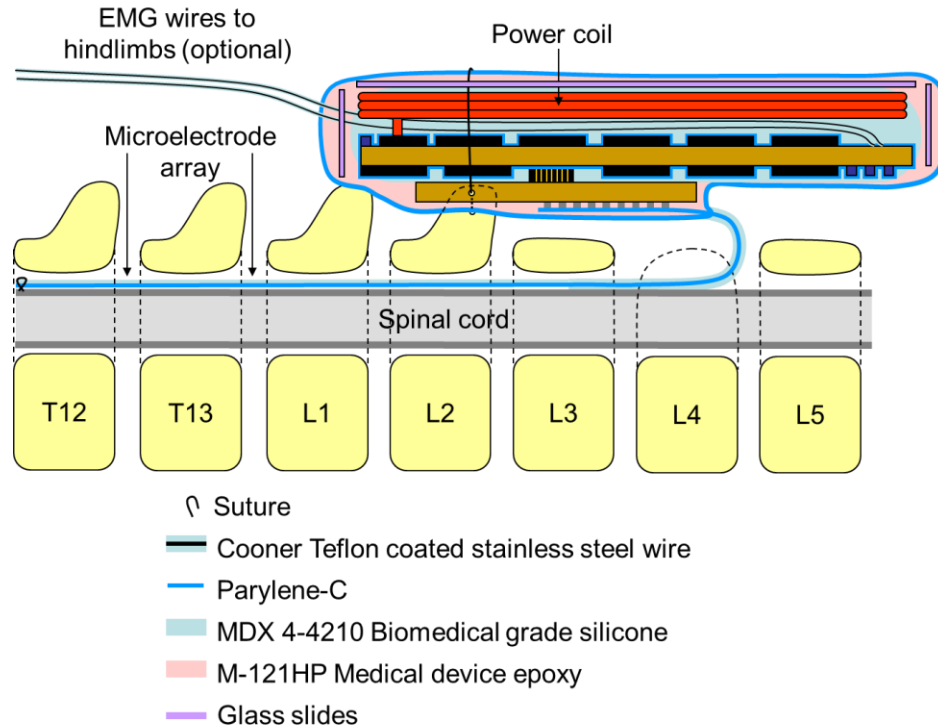


Figure 4.10: Illustration of the wireless array implant after implantation, and photograph of the complete implant

The wireless implant is fundamentally an evolution of the multiplexed implant. Figure 4.10 shows how the implant will be placed inside the rat next to the spinal cord. One important improvement was made in the encapsulation process, where pieces of glass cut from slides were embedded into the packaging to further reduce leakage. The high Q coil and antenna's balun/matching circuit (for data transmission) is very sensitive to leakage, and early prototypes suggested that the previous encapsulation method was insufficient.

4.5.1 System Overview

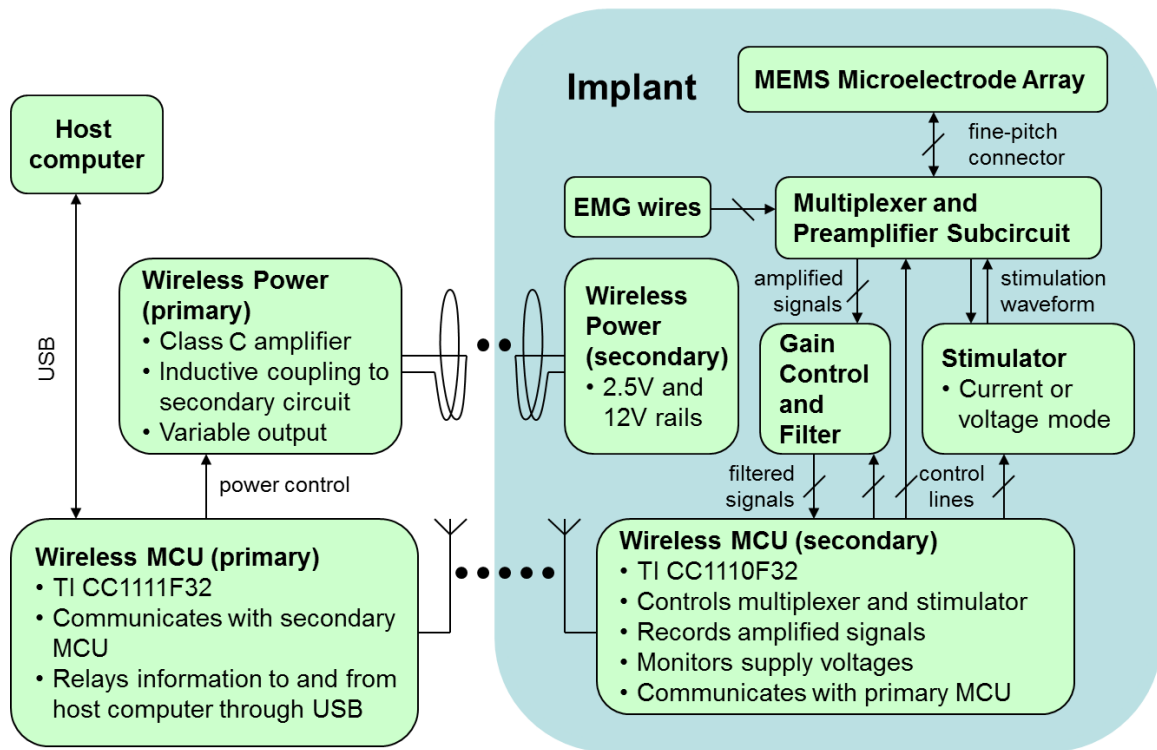


Figure 4.11: Block diagram for the wireless implant system.

Illustrated in figure 4.11 is the block diagram of the wireless implant system. The multiplexer circuit is the same as that illustrated in figure 3.4a, except its signal lines are now interfaced with a MCU as opposed to going to the headplug. The other components of the implant are described in the sections below. The gain control and filter is used for recording, and described in section 4.5.2.1. The stimulator circuit, described in section 4.5.2.2, takes digital signals from the MCU and generates an analog waveform. The wireless power circuit is that shown in figure 4.9.

On the primary side, there is a host computer connected to a CC1111F32 via USB. It has software written in C++ to present a user interface that controls the wireless

implant. Each action sends a command to the CC1111F32, which then relays the command wirelessly to the CC1110F2 in the implant (unless it is a command intended for the primary side only), which in turn will send the appropriate signals to the multiplexer and stimulator circuits. The programs running on both MCUs (written in C and compiled to microcode using IAR Embedded Workbench) coordinates wireless communication between each other, switching between transmit and receive mode as required, and adjusting transmit power depending on how strong the signal was for the other side.

4.5.2 Wireless Microprocessor Transceiver Circuit

At the core of the wireless implant is a CC1110F32 microprocessor transceiver SoC from Texas Instruments. The processor core is based on the 8051 instruction set and runs at 26MHz, and it has a versatile DMA engine to offload data transfer from the MCU. The transceiver is operates in sever ISM radio bands, the highest being 782-928 MHz. This chip was chosen over 2.4 GHz variants to avoid possible interference with ubiquitous consumer devices operating in that band. The circuit for the SoC is shown in figure 4.12.

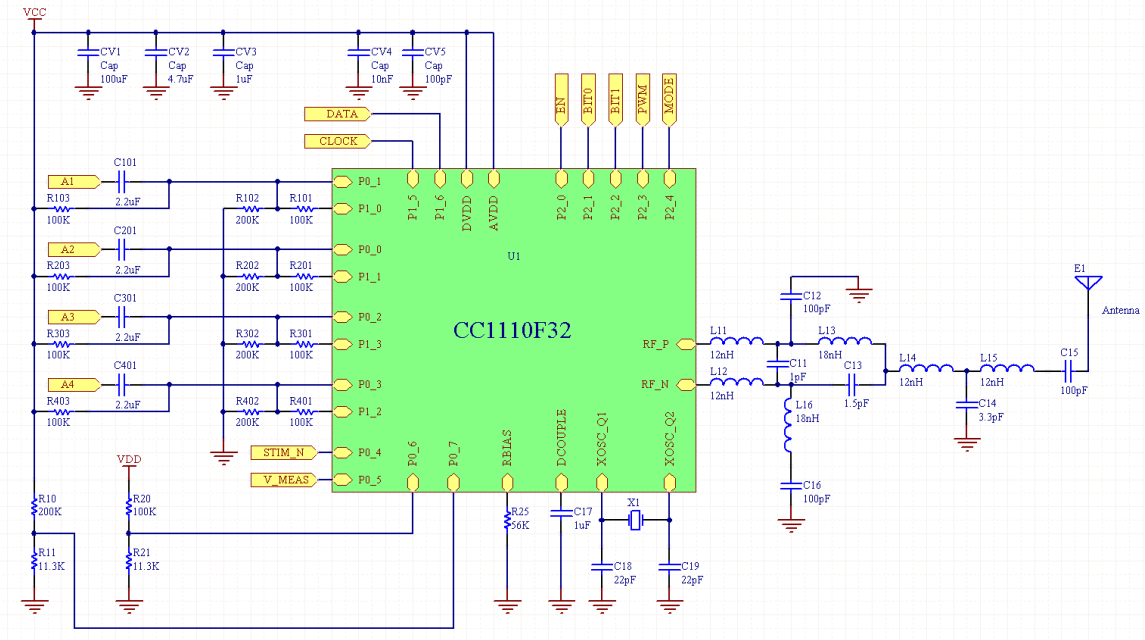


Figure 4.12: Schematic for the microprocessor transceiver circuit

4.5.2.1 Recording

The CC1100FX is equipped with a Delta-Sigma Modulator based analog to digital converter. At the fastest sampling rate of 54 kSamples per second, it has 7-bit accuracy. Up to 8 pins on the processor can be used for analog input, but they are done sequentially. Lower sampling speeds can increase the accuracy up to 12-bit. The implant uses the ADC to record the signals from the analog signal lines A1-A4 coming from the multiplexer circuit, as seen on the left side of Figure 4.12.

A high-pass filter circuit with offset ability appears at each input. Consider the RC network around input A1. Pin P0_1 is an input to the ADC, and has 200k Ω input impedance, while Pin P1_0 is a digital output. Because the ADC is incapable of reading negative voltages, the filter applies a DC offset to the AC signal coming through the

capacitor C101, and that offset will depend on P1_0. A low offset also allows the ADC to use a smaller reference voltage, improving the ability to read smaller signals.

4.5.2.2 Stimulation

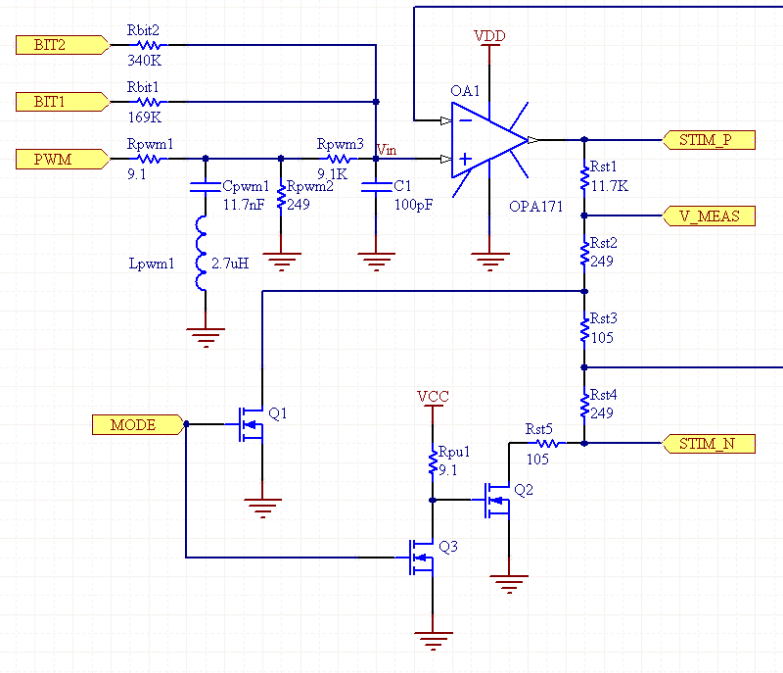


Figure 4.13: Stimulator subcircuit

The stimulator circuit is similar to the one found in the control box used with the multiplexed implant, and its schematic is shown in Figure 4.13. A PWM signal is controlled by a hardware timer with a period of 31 cycles (corresponding to a frequency of 838 kHz), allowing 32 values for the duty cycle (0 to 31 cycles). The carrier frequency of the PWM signal gets filtered with a notch filter (Cpwm1 and Lpwm1, $Q=10$), and the remaining components of the PWM signal goes to a low pass filter (C1 and Rpw3, $t_{RC}=9\mu\text{s}$) along with two digital outputs from BIT0 and BIT1, for a total of 128 different analog voltages at the positive input of the op amp. A digital MODE signal controls

MOSFETs Q1-Q3 determines how the op amp circuit will behave. If Mode is low, Q1 is closed while Q2 is open, and the circuit will behave like a non-inverting amplifier and the stimulator will output constant voltage pulses. If Mode is high, Q1 is open while Q2 is closed, and the circuit will behave like a voltage-to-current amplifier and the stimulator will output constant current pulses. The software is able to control the PWM, BIT0, and BIT1 signals with roughly $2\mu\text{s}$ timing accuracy.

4.5.3 Power Regulation Daughterboard

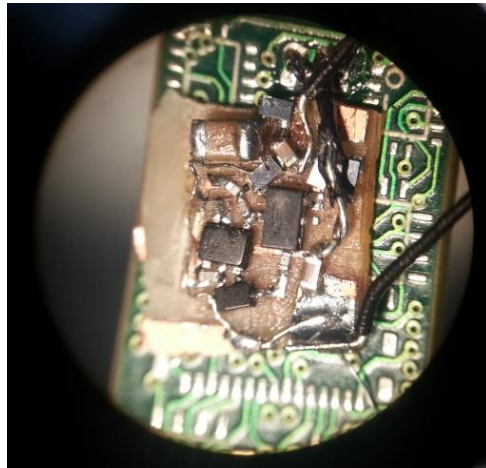


Figure 4.13: Daughterboard containing the power delivery control circuit.

The power delivery from the coil is controlled using the circuit in figure 4.9, although the necessity of this stage was foreseen at the time of PCB design. As it would be exceedingly difficult to redesign the PCB give the size constraints, the circuit was implemented on a daughterboard, as shown in Figure 4.14.

4.6 Results

The wireless implant has been almost perfectly functional in a benchtop setting. When the implant is brought within 5.2 cm of the primary coil, the wireless power system is able to provide power to all the subsystems, which in turn all function as intended. Using a software interface similar to that shown in section 3.3.6, the host computer can send commands to the CC1111F32 primary microprocessor transceiver via USB and also read data back from it. The CC1111F32 is also able to wirelessly send commands to the CC1110F32 in the implant as well as wirelessly receive data from the implant. From these commands, the CC1110F32 is able to send the appropriate configuration code to the multiplexer subcircuit as described in section 3.3.3, and it provides the correct input signals (PWM, BIT0, and BIT1) to the stimulator circuit described in section 4.5.2.2 to generate the desired stimulation waveform.

Depending on the orientation and separation of the devices, wireless commands from the sender (whether originating from the CC1111F32 or the CC1110F32) on occasion were not received by the receiver, but such packet loss is to be expected in real world wireless systems. To handle this, the microcode on the wireless microprocessors is written such that immediately after the CC1111F32 sends a command, it is temporarily put into receive mode to receive an acknowledgement signal from the CC1110F32 in the implant. Correspondingly, immediately after the CC1110F32 receives a message, it is temporarily put into transmit mode to send the acknowledgement message. If the CC1111F32 does not receive the acknowledgement packet within 10 μ s, the original command is resent. The acknowledgement message can also contain recording data.

A full test of the final implant in-vivo was unable to be completed, but preliminary testing of a prototype was. To minimize the possibility of failure, the prototype was equipped with a pair of wires for stimulation as opposed to a microelectrode array, with the wires affixed to two pads on the array daughterboard, and instead of the implant being fixed to the spine as in figure 4.10, it was placed just under the skin, as can be seen in Figure 4.14. The stimulation wires were sutured to the dura of the spinal cord. This approach brought the wireless implant's electronic package away from the interior of the rat, reducing the distance and mass of tissue between the implant and the primary coil & transceiver.



Figure 4.14: Rat with wireless implant prototype just under the skin

The first attempt achieved wireless power transmission and data connectivity after implantation and rat healing, and according to the recording of the stimulation waveform

read by the microprocessor (on the V_MEAS signal), the stimulator subcircuit was outputting the correct stimulation waveform. Connectivity was maintained with a separation distance of up to 44mm from the skin surface to the plane of the primary coil. However, the rat did not show any biological response indicative of stimulation to the spinal cord. After 15 days, this behavior persisted, so the animal was terminated and the implant was removed for analysis. Using an oscilloscope, it was found that the stimulation wires (along with the PCB traces they were connected to) did not have a voltage waveform output across them. This suggested that there was a problem between the stimulator and the wires, namely the multiplexer circuit. After selective removal of the package encapsulation, the final bit of the shift register was probed, and the waveform showed expected output for various configuration codes. Since the shift registers are daisy chained, this showed that all of them functioned correctly. Custom configuration codes for the multiplexer circuit then isolated the issue to a malfunction of multiplexer M0. It is not clear what caused the chip to fail, but possible modes of failure seen in the past include loss of connection between the chip pads and the PCB due to poor soldering from the assembler. A loose resistor in a different part of the circuit was also found that occasionally resulted in erratic voltage recording. It is suspected that the encapsulation process and heat cycles from curing may place stress on solder joints, as the sealing materials flow into the small space beneath chips and the PCB, and have different expansions coefficients than the PCB and its components.

Since the rest of the implant was functional, new stimulation wires were soldered directly to the stimulator subcircuit of this same implant, bypassing the multiplexer circuit, and after encapsulation it was reimplanted in another rat. This time, the implant

was fully functional, showing hindlimb movement when the spinal cord was stimulated.

Figure 4.16 shows a screenshot of the software interface, with a voltage waveform readback from the implant during stimulation. Figure 4.17 shows a frame from a video of the rat's responses to low frequency 5V stimulation pulses. Functionality was retained after four weeks.

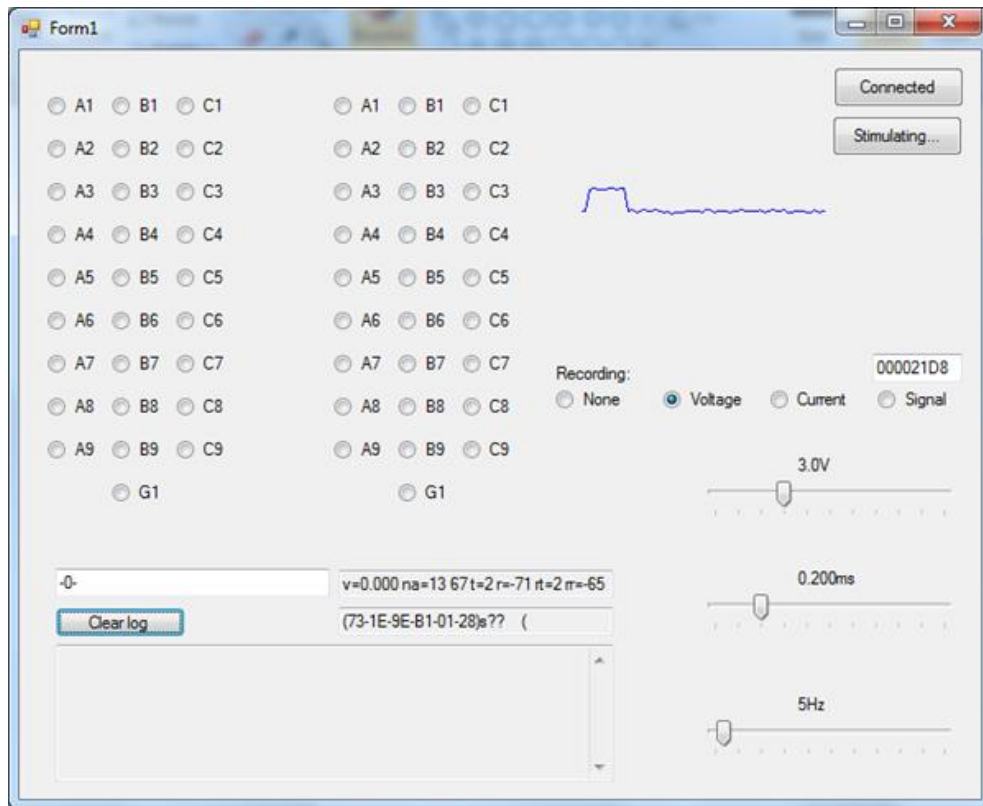


Figure 4.16: Software user interface showing voltage waveform recording.



Figure 4.17: Photograph of the wireless implant inducing hindlimb motion in a spinalized rat.

4.7 Summary

A wireless microelectrode array implant system was designed, built, and tested on the benchtop. Although the full design was unable to be tested in vivo, a prototype consisting of the same electronics package that used two wires for stimulation (as opposed to the microelectrode array) was proven to be functional after four weeks inside a rat, and was able to stimulate the spinal cord.

The new subsystems required for the wireless implant were all verified to function in vivo. A wireless power system delivered the power required for the implant to operate. A stimulator circuit was able to generate the desired stimulation waveform with all the parameters of the previous system with external stimulator. The SoC was able to record the stimulation waveform and transmit the data to the host computer.

The work in this chapter is a proof of concept illustrating the viability of practical wireless implants for chronic in-vivo experiments using only inexpensive polymers and glass slides for encapsulation alongside off-the-shelf ICs in the electronics.

5. References

- [1] Christopher and Dana Reeve Foundation. "One Degree of Separation: Paralysis and Spinal Cord Injury in the United States."
http://www.christopherreeve.org/site/c.ddJFKRNoFiG/b.5091685/k.58BD/One_Degree_of_Separation.htm
- [2] Neurosurgerytoday.org. "Spinal cord injury."
http://www.neurosurgerytoday.org/what/patient_e/spinal.asp
- [3] L. J. Noble and J. R. Wrathall. "Correlative analyses of lesion development and functional status after graded spinal-cord contusive injuries in the rat."
Experimental Neurology 103 (1989): 34-40.
- [4] National Institute of Neurological Disorders and Stroke, National Institutes of Health. "Spinal cord injury: Hope through research."
http://www.ninds.nih.gov/disorders/sci/detail_sci.htm
- [5] Grillner, S. "Locomotion in vertebrates: Central mechanisms and reflex interaction." *Physiological Reviews* 55 (2): 247–304. 1975.
- [6] J. H. Burridge, P. N. Taylor, S. A. Hagan, D. E. Wood, and I. D. Swain. "The effects of common peroneal stimulation on the effort and speed of walking: A randomized controlled trial with chronic hemiplegic patients," *Clinical Rehabilitation* 11 (3): 201-210. Aug 1997.
- [7] K. W. Horch and G. S. Dhillon. *Neuroprosthetics theory and practice*. River Edge, NJ, USA: World Scientific, 2004.

- [8] P. S. Shurrager and R. A. Dykman. "Walking spinal carnivores." *Journal of Comparative and Physiological Psychology* 44 (3): 252-262. 1951.
- [9] R. D. de Leon, J. A. Hodgson, R. R. Roy, and V. R. Edgerton. "Full weight-bearing hindlimb standing following stand training in the adult spinal cat." *Journal of Neurophysiology* 80 (1): 83-91. Jul 1998.
- [10] E. C. Field-Fote. "Spinal cord control of movement: Implications for locomotor rehabilitation following spinal cord injury." *Physical Therapy* 80 (5): 477-484. May, 2000.
- [11] S. Grillner. "Neurobiological bases of rhythmic motor acts in vertebrates." *Science* 228 (4696): 143-148. Apr 1985.
- [12] T. Flash and B. Hochner. "Motor primitives in vertebrates and invertebrates." *Current Opinion in Neurobiology* 15 (6): 660-666. Dec 2005.
- [13] M. C. Tresch and O. Kiehn. "Population reconstruction of the locomotor cycle from interneuron activity in the mammalian spinal cord." *Journal of Neurophysiology* 83 (4): 1972-1978. Apr 2000.
- [14] Edgerton V, Tilakaratne N, Bigbee A, de Leon R and Roy R. "Plasticity of the spinal neural circuitry after injury." *Annual Review of Neuroscience* 27 (2004): 145-167.
- [15] Hodgson JA, Roy RR, de Leon R, Dobkin B, Edgerton VR. "Can the mammalian lumbar spinal cord learn a motor task?" *Medicine & Science Sports Exercise* 26 (1994): 1491-1497.

- [16] Forssberg H. “Stumbling corrective reaction: a phase-dependent compensatory reaction during locomotion.” *Journal of Neurophysiology* 42 (4):936-953. 1979.
- [17] Musienko, P., Courtine, G., Tibbs, J.E., Kilimnik, V., Savochin, A., Roy, R.R., Edgerton, V.R., and Gerasimenko, Y. “Somatosensory control of balance during locomotion in decerebrated cat.” *Journal of Neurophysiology* 107 (8): 2072-82. Apr 2012.
- [18] Gerasimenko YP, Avelev VD, Nikitin OA, Lavrov IA. “Initiation of locomotor activity in spinal cats by epidural stimulation of the spinal cord.” *Neuroscience and Behavioral Physiology* 33 (2003): 247–254.
- [19] Gerasimenko YP, Ichiyama RM, Lavrov IA, Courtine G, Cai L, Zhong H, Roy RR, and Edgerton VR. “Epidural spinal cord stimulation plus quipazine administration enable stepping in complete spinal adult rats.” *Journal of Neurophysiology* 98 (2007): 2525–2536.
- [20] Ichiyama RM, Gerasimenko YP, Zhong H, Roy RR, Edgerton VR. “Hindlimb stepping movements in complete spinal rats induced by epidural spinal cord stimulation.” *Neuroscience Letters* 383 (2005): 339–344.
- [21] Lavrov, I, Courtine G, Dy CJ, van den Brand R, Fong AJ, Gerasimenko YP, Zhong H, Roy, RR, and Edgerton VR. “Facilitation of stepping with epidural stimulation in spinal rats: role of sensory input.” *Journal of Neuroscience* 28 (2008): 7774–7780.
- [22] Harkema S, Gerasimenko YP, Hodes J, Burdick J, Angeli C, Chen Y, Ferreira C, Willhite A, Rejc E, Grossman R and Edgerton VR. “Effect of epidural stimulation

- of the lumbosacral spinal cord on voluntary movement, standing and assisted stepping after motor complete paraplegia: a case study." *The Lancet* 377 (2011): 1938-1947.
- [23] Difrancesco, D. "Pacemaker Mechanisms in Cardiac Tissue." *Annual Review of Physiology* 55 (1993): 455-472.
- [24] Altman, Lawrence K. "Arne H. W. Larsson, 86; Had First Internal Pacemaker." *NY Times*, Jan 18, 2002.
- [25] Mirowski, M. "The Automatic Implantable Cardioverter-Defibrillator – An Overview," *Journal of the American College of Cardiology* 6 (1985): 461-466.
- [26] M. S. Humayun, J. D. Weiland, G. Y. Fujii, R. Greenberg, R. Williamson, J. Little, *et al.* "Visual perception in a blind subject with a chronic microelectronic retinal prosthesis." *Vision Research* 43 (2003): 2573-2581.
- [27] F. Strumwasser, *Science* 127 (1958): 469–470.
- [28] CA Thomas, PA Springer, GE Loeb, Y Berwald-Netter, LM Okun. "A miniature microelectrode array to monitor the bioelectric activity of cultured cells." *Exp Cell Res* 74 (1972): 61-66.
- [29] K.D. Wise, J.B. Angell, and A. Starr. *IEEE Transactions on Biomedical Engineering BME-17* (1970): 238–247.
- [30] K.D. Wise and J.B. Angell. *IEEE Transactions on Biomedical Engineering BME-22* (1975): 212–219.
- [31] G. S. Wilson and R. Gifford. "Biosensors for real-time in vivo measurements." *Biosensors and Bioelectronics* 20 (2005): 2388-2403.

- [32] PJ Chen, DC Rodger, S Saati, MS Humayun, YC Tai. "Microfabricated implantable parylene-based wireless passive intraocular pressure sensors." *Journal of Microelectromechanical Systems* 17(6): 1342-1351. Oct 2008.
- [33] Y. Haga and M. Esashi. "Biomedical microsystems for minimally invasive diagnosis and treatment." *Proceedings of the IEEE* 92 (2004): 98-114.
- [34] Y. Yoon, G. S. Lee, K. Yoo, and J. B. Lee. "Fabrication of a Microneedle/CNT Hierarchical Micro/Nano Surface Electrochemical Sensor and Its In-Vitro Glucose Sensing Characterization." *Sensors* 13 (2013): 16672-16681.
- [35] T. Stieglitz, H. È. Beutel, M. Schuettler, J. U. Meyer. "Micromachined, Polyimide-Based Devices for Flexible Neural Interfaces." *Biomedical Microdevices* 2(4): 283-294. Dec 2000.
- [36] "Parylene knowledge: discovery / history," Specialty Coating Systems.
- [37] J. Noordegraaf, "Conformal coating using parylene polymers," *Medical device technology* 8 (1997): 14-20.
- [38] G. E. Loeb, M. J. Bak, M. Salcman, and E. M. Schmidt. "Parylene as a Chronically Stable, Reproducible Microelectrode Insulator." *Ieee Transactions on Biomedical Engineering* 24 (1977): 121-128.
- [39] Wolgemuth L. "Assessing the performance and suitability of parylene coating." *Medical Device and Diagnostic Industry* 22 (2000): 42-49.
- [40] Tai, Y. C. "Parylene MEMS: material, technology and applications." *Proceedings of the 20th Sensor Symposium* (2003): 1-8.

- [41] Wise, K. D. "Silicon microsystems for neuroscience and neural prostheses." *IEEE Engineering in Medicine and Biology Magazine* 24(5): 23-29. Sept 2005.
- [42] C. Pang. "Parylene technology for neural probes applications." PhD diss., California Institute of Technology, 2007.
- [43] Rodger DC, and Tai YC. "Microelectronic packaging for retinal prostheses." *IEEE Engineering in Medicine and Biology Magazine* 24 (2005): 52-57.
- [44] Rodger DC, Weiland JD, Humayun MS, and Tai YC. "Scalable high lead-count parylene package for retinal prostheses." *Sensors and Actuators B-Chemical* 117 (2006): 107-114.
- [45] Kovacs GTA. "Introduction to the Theory, Design and Modeling of Thin-Film Microelectrodes for Neural Interfaces". In *Enabling Technologies for Cultured Neural Networks*, edited by Stenger DA and McKenna T, 121-166. Academic Press, 1994.
- [46] Roy RR, Hodgson JA, Lauret SD, Pierotti DJ, Gayek RJ, and Edgerton VR. "Chronic spinal cord-injured cats: surgical procedures and management." *Laboratory Animal Science* 42 (1992): 335-343.
- [47] Roy RR, Hutchison DL, Pierotti DJ, Hodgson JA, and Edgerton VR. "EMG patterns of rat ankle extensors and flexors during treadmill locomotion and swimming." *Journal of Applied Physiology* 70 (1991): 2522-2529.
- [48] Edgerton VR, McCall GE, Hodgson JA, Gotto J, Goulet C, Fleischmann K, and Roy RR. "Sensorimotor adaptations to microgravity in humans". *Journal of Experimental Biology* 204 (2001): 3217-3224.

- [49] Nandra MS, Lavrov IA, Edgerton VR and Tai YC. “A Parylene-based microelectrode array implant for spinal cord stimulation in rats.” *Proceedings of the 24th IEEE Conference on Micro Electro Mechanical Systems (MEMS 2011)*: 1007-1010.
- [50] Courtine G, Gerasimenko YP, van den Brand R, Yew A, Musienko P, Zhong H, Song B, Ao Y, Ichiyama RM, Lavrov IA, Roy RR, Sofroniew MV, and Edgerton VR. “Transformation of nonfunctional spinal circuits into functional states after the loss of brain input.” *Nature Neuroscience* 12 (2009): 1333–1342.
- [51] Gad P, Choe J, Nandra MS, Zhong H, Roy RR, Tai YC and Edgerton VR. “Development of a multi-electrode array for spinal cord epidural stimulation to facilitate stepping and standing after a complete spinal cord injury in adult rats.” *Journal of NeuroEngineering and Rehabilitation* 2013, 10:2.
- [52] Vejsada R and Hnik P. “Radicular innervations of hindlimb muscles of the rat.” *Journal of Physiology and Biochemistry* 29 (1980): 385-392.
- [53] Nicola Tesla, “The transmission of electrical energy without wires”, *Electrical World and Engineer*, March 1905.
- [54] Schuder, J.C., Stephenson, H.E. Jr., and Townsend, J.F. “High-level electromagnetic energy transfer through a closed chest wall.” *I.R.E. Internat. Convention Rec.* 9 (1961): 119.
- [55] W. H. Ko, S. P. Liang, and C. Fung. “Design of radio-frequency powered coils for implant instruments.” *Med. Biol. Eng. Comput.* 15 (1977): 634–640.

- [56] A.B. Kurs, A. Karalis, R. Moffatt, J.D. Joannopoulos, P.H. Fisher, and M. Soljacic. "Wireless Power Transfer via Strongly Coupled Magnetic Resonances." *Science* 317 (2007): 83-86.
- [57] N. O. Sokal and A. D. Sokal. "Class-E- A New Class of High-Efficiency Tuned Single-Ended Switching Power Amplifiers." *IEEE J. Solid-State Circuits* 10 (1975): 168-176.